Applied Physics Reviews REVIEW scitation.org/journal/are

Emerging tunable window technologies for active transparency tuning

Cite as: Appl. Phys. Rev. 9, 031304 (2022); doi: 10.1063/5.0089856
Submitted: 1 March 2022 · Accepted: 14 July 2022 ·
Published Online: 18 August 2022

View Online Export Citation CrossMark

M. Shrestha,[1,a] G. K. Lau,[2] A. K. Bastola,[3] Z. Lu,[4] A. Asundi,[5] and E. H. T. Teo[6]

AFFILIATIONS

[1]Continental-NTU Corporate Lab, Nanyang Technological University, Singapore 639798
[2]Department of Mechanical Engineering, National Yang Ming Chiao Tung University, Hsinchu 30010, Taiwan
[3]Centre for Additive Manufacturing, School of Engineering, University of Nottingham, Nottingham NG8 1BB, United Kingdom
[4]School of Aeronautics and Astronautics, Sun Yat-Sen University (Shenzhen Campus), 518107, Shenzhen China
[5]d'Optron Pvt. Ltd., 71 Nanyang Drive, Singapore 638075
[6]School of Electrical and Electronic Engineering and School of Materials Science and Engineering, Nanyang Technological University, Singapore 639798

[a)]Author to whom correspondence should be addressed: milan001@e.ntu.edu.sg

ABSTRACT

Most modern high-rise buildings' facades use glasses for esthetics, daylight, and better environmental view through them. However, with the increasing use of a larger area of transparent glasses as walls, the visual privacy preservation of the indoors and heat energy loss through the windows are becoming a rising concern. Recent studies showed that nearly half of the energy consumed in a building goes to heating and air conditioning while approximately 40% of this energy is lost through windows. Windows with tunable optical properties that are generically termed "tunable windows or smart windows or switchable glass" are perceived as a potential solution for these problems. An optically tunable window can adjust the amount of daylighting passing through it, control the heat radiation, and/or change the transparency of the glasses for visual privacy preservation of indoors. Electrochromic glasses, polymer dispersed liquid crystal glasses, and suspended particle devices are available as commercial tunable windows but their high cost, limited optical performance, reliability, and operational complexity are hindering the widespread adaptation. Therefore, several other technologies for low-cost actively tunable windows capable of actively adjusting transparency are increasingly explored. However, most of such new technologies, working based on various optical principles, do not fulfill all the requirements of tunable windows. For instance, some can tune optical transmittance but do not affect energy transmission, and some can adjust heat radiation transmission but has a limited change in visual appearances. To fully take the advantage of the strengths as well as recognize the limitations of such emerging technologies, their optical principles need to be understood in-depth. Here, we review the recent developments in transmittance tunable windows by categorizing them based on the optics involved, namely, light absorption, reflection, and scattering. This in-depth review comprehensively discusses how the tunable window technologies compare to each other and offers insight into how their performance can be improved in the future.

TABLE OF CONTENTS

I. OVERVIEW OF TUNABLE WINDOWS AND THEIR SIGNIFICANCE

Energy used for heating and air conditioning (HVAC) accounts for more than 45% of buildings' energy consumption.[1–4] Recent studies based in Norway and China showed such high energy required for

HVAC is majorly attributed to the energy loss through windows, which is over 40% of total building energy loss.[5–7] However, the windows in the buildings are unavoidable but a necessity due to civilization evolvement—windows allow daylight to the building as well as allow occupants comfort by providing visual contact with their surroundings. Transmittance tunable windows or energy-efficient windows, sometimes referred to as smart windows, are one of the increasingly popular developments to reduce the energy consumption in buildings for the reason that such windows offer abilities to modulate the throughput of daylight for illumination and solar energy for heating/cooling.[8–13] Such an effect—to modulate the throughput of daylight and solar energy through windows—can be attained by many different approaches, and a well-studied and commercially available example includes the use of chromic material, a functional material that exhibits a distinct color change when exposed to an external stimulus.[1,14–17] In general, chromic materials can be distinguished as photo-chromic,[13,16,18,19] thermo-chromic,[15,17,20–22] and electro-chromic[23–27] depending on the external stimuli such as light, heat, and electricity, respectively.[28,29] Moreover, other tunable materials such as suspended particle devices (SPD) and polymer dispersed liquid crystal devices (PDLC)[30–33] are also used to develop commercial transmittance tunable windows.

The optically tunable materials (e.g., chromic) modulate the energy flux of solar energy through windows by improving either their absorbance or reflectance.[14,34–36] Therefore, energy-saving can be obtained via such modulations—for example, a window can be more transparent during the sunshine allowing solar energy into the building (in winter where the heating system is running) or be opaquer during the sunshine blocking the solar energy into the building (in summer where air conditioning system is running). On the other hand, the occupant's thermal comfort—use to manifest the thermal state of a person in a given environment[37,38]—is directly determined by an ambient temperature, which is completely controlled by energy input/output into the building [Fig. 1(a)]. Thus, the integration of actively controllable tunable materials into windows not only allows the adjustment of daylight and solar energy into the buildings offering energy saving but also helps in occupants' comfort. With such stimulating features—beneficial in both energy saving as well as human comfort—new technologies for actively tunable windows are extensively explored, in recent decades.

Other energy-saving approaches include the use of thermoelectric materials and photoelectrochromic materials in windows. Transparent thermoelectric materials are employed to harvest heat energy dissipating through windows.[39,40] Meanwhile, the photoelectrochromic materials enable change in optical transmittance of the windows while simultaneously harvesting solar energy into electrical energy. Hence, photoelectrochromic materials promise self-powered transmittance tunable windows capable of sustainable operation without the need for external energy.[41–45] Current photoelectrochromic devices (PECDs) can achieve moderate optical modulation (<70%) and a photoconversion efficacy of ∼7%. These PECDs typically consist of a dye-covered nanostructured layer such as a TiO_2 layer on a porous tungsten trioxide (WO_3) anode deposited onto a conductive glass, while the iodine (I^{-1}/I^{-3}) solution acts as a redox mediator (electrolyte) and a thin platinum film as a counter electrode (CE).[43,46] The CE and redox mediator are considered the most critical components of PECDs. Therefore, to enhance the performance of PECDs, alternative materials for efficient and stable CE and redox media are being developed. For instance, a recent study (2021) reported graphene nanoplatelets as alternative corrosion resistance and stable CE and copper (I/II) complexes—abundant (as well as cheaper) raw material—as an alternative electrolyte.[46]

In all of these energy-efficient tunable window approaches, the main goals are to cut down costs and enhance the overall efficiency of the device performance using various innovative materials and structural designs.[8,9,35,47–51] Although several technologies for low-cost tunable windows capable of actively adjusting optical transmittance are increasingly explored, all these technologies with variations in working optical principles cannot fulfill all of the functionalities of tunable windows. For instance, some can tune optical transmittance but do not affect energy transmission, and some can adjust heat radiation transmission but has a limited change in visual appearances. To fully understand the strengths and limitations of such tunable windows, their optical principles need to be studied in-depth. Therefore, this article aims to delineate an assessment of emerging technologies for actively tunable windows by categorizing them based on their working optical principles, (i) absorption, (ii) reflection, and (iii) diffuse transmission or scattering as shown in Figs. 1(c)–1(e).

A transmittance tunable window can adjust the specular transmittance by manipulating the reflection and absorption or even by the diffuse transmission of incident light. For example, SPD or electrochromic glass is known for tuning the optical absorbance and, therefore, it can adjust the optical transmittance;[52,53] whereas, the thickness change in the optical absorbing material can also alter the optical transmittance.[54–56] On the other hand, optofluidic glasses tune reflection to alter the transmittance.[57] Similarly, forward light scattering or light diffusion can reduce optical clarity. For instance, PDLC becomes hazy when the light is scattered through the boundaries between the polymeric matrix and liquid crystal droplets (having a random refractive index).[58–60] However, it can switch back to clear when the liquid crystal droplets are rearranged with a normal refractive index similar to that of the polymeric matrix's refractive index. Moreover, the transparent optical media having rough surfaces can disperse light in a random optical path—known as an optical phase. For instance, flat glass is clear; however, ground glass looks hazy. Therefore, tuning the surface roughness offers a method to develop adjustable optical diffusive devices, which can adjust the specular optical transmittance.[60–68] Tunable windows that work based on light absorption and reflection have more impact on energy transmission through the windows, but they might not be able to obtain complete opaqueness for privacy preservation. Meanwhile, those working on diffuse transmission will have good visual privacy preservation applications but might not be efficient to control radiation transmission in the building.

To understand the potential application and effectiveness of these categories of tunable windows, a better understanding of the light and material interaction is required. Once the light beam incident on optical media, it is partly reflected, absorbed, and transmitted [Fig. 1(b)].[69–71] As given in Eq. (1), the ratio of the reflected, absorbed, and transmitted light to incident light intensity is known as reflectance (R), absorbance (A), and transmittance (T), respectively,

$$R + A + T = 1. \tag{1}$$

Equation (1) implies that the optical transmittance changes in accordance with the change in reflectance and absorbance. The tunable

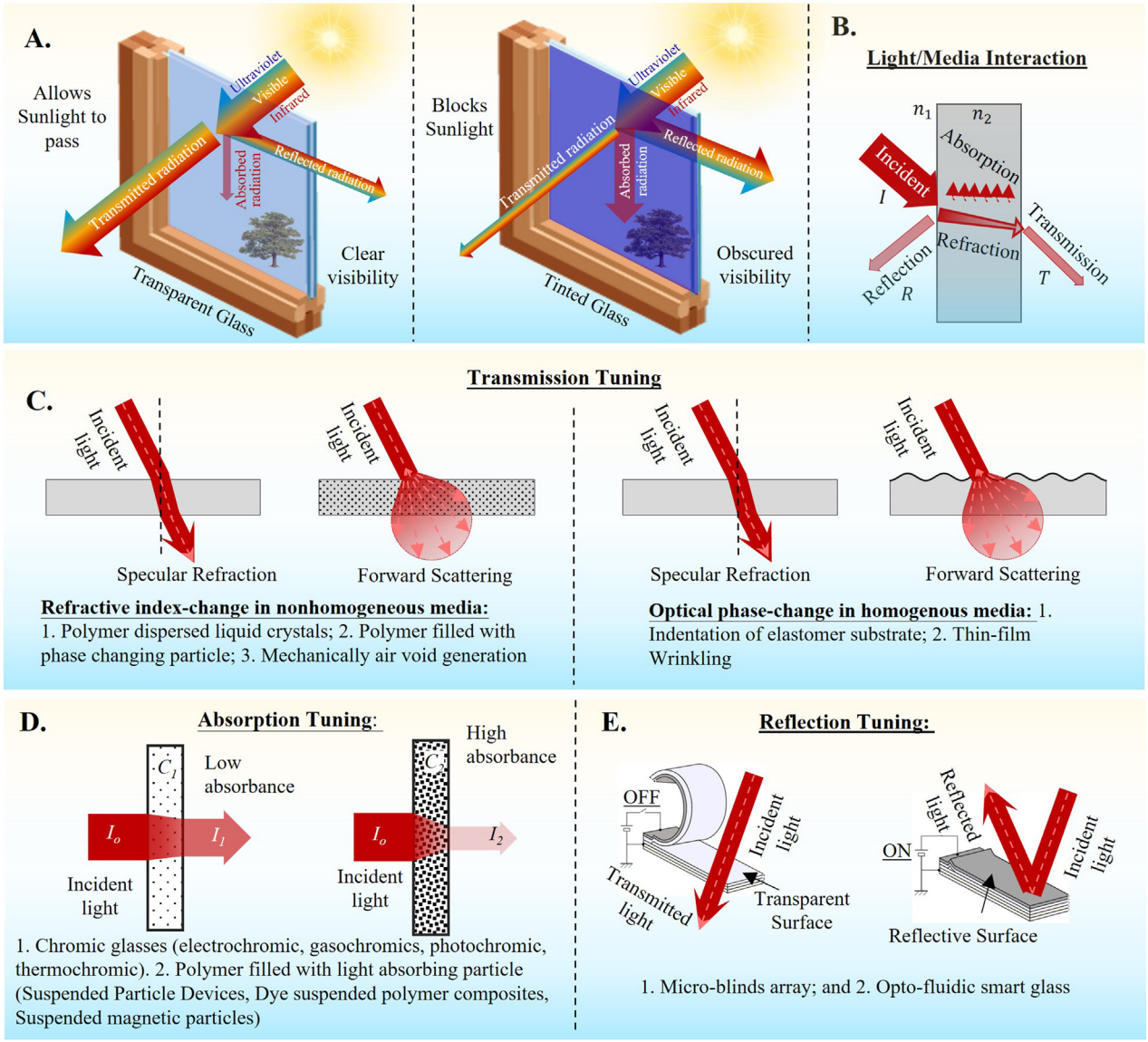

FIG. 1. (a) Illustration of an actively switchable window showing the interaction of solar radiation with transparent glass and clear visibility through it (left); interaction of solar radiation with a darkened or tinted glass and poor visibility through it (right); (B) schematics showing the basic interaction of light and materials; illustration of the actively switchable windows for transmittance tuning that are categorized based on basic optical principles: (C) transmission tuning; (D) absorption tuning; and I reflection tuning.

windows' performance is generally quantified in terms of optical transmittance (inline or specular) due to the ease of measurement. The transmittance is identified as $T_{spec} = \frac{I_{spec}}{I_o}$, where I_{spec} is the intensity of transmitted light and I_o is the intensity of incident light. A transmittance $T_{spec} = 1$ implies the perfect optical clarity, and $T_{spec} = 0$ implies a complete opacity.

In this review, we present a comprehensive overview of various types of transmittance tunable window technologies. An insight into different types of tunable windows can be gained by understanding the optical principles involved. Henceforth, we categorized such tunable windows technologies based on the optics involved and further sub-categorized them based on the stimulus required to achieve dynamic properties, for the first time. Although there are a few transmittance tunable windows available in the market, currently, their high cost is the biggest weakness to getting a wider adaptation.[72–76] On the other hand, the current state-of-the-art technologies as highlighted in this review show potential as an alternative for the tunable window devices for the future. In the following, we first briefly discuss the commercially available tunable windows. Thereafter, we comprehensively present the emerging technologies for transmittance tunable window devices—therein, such technologies are categorized based on the optical principle involved.

II. COMMERCIALLY EXISTING ACTIVELY TUNABLE WINDOW TECHNOLOGIES

Optical transmittance tunable window devices have been available in the market for more than a decade. These commercially available tunable windows are based on (or a combination of) electrochromic glasses or PDLC or SPD technology. There are used cases in cars, airplanes, trains passing close to residential areas-/corporate buildings, and so on.[72,77–79] To distinguish the emerging transmittance tunable window technologies in terms of working principles, these commercially available window devices are briefly introduced in this section.

Various electrochromic glasses-based transmittance tunable windows are currently available in the market.[80–82] These electrochromic glasses can change color in the presence of an external electric field and, thus, can tune the quantity of light absorption.[54–56] Electrochromic glasses comprise an electrochromic layer, ion storage layer, and electrode packed in between conductive and transparent layers [Fig. 2(a)]. The basic electrochromic layers are created using inorganic materials—common examples include oxides of nickel and tungsten.[52,83] Furthermore, other organic compounds such as anthraquinones, viologens, tetrathiafulvalenes, and diphthalocyanines are were also utilized to create the electrochromic layer.[84] The inorganic electrochromic material shifts its color when ions, such as H^+ and Li^+, are introduced or removed using an external electric field. On the other hand, organic electrochromic materials achieve coloration by oxidation–reduction reaction.[85] Currently, it can be found that electrochromic glasses are developed to an industry-ready state with a transmittance tuning range of 60%–70%.[86] However, the major challenges for widespread adaptation remain in cost and reliability (with UV light exposure).

Polymer dispersed liquid crystal devices (PDLC) based tunable window appliances are the most common product, that is, commercially available in the market.[87–90] PDLC tunes the light scattering, which switches its appearance from hazy to clear in the presence of an external electric field.[84,91,92] PDLC is a composite material and comprises micrometer-sized liquid crystal droplets diffused within the polymeric matrix [Fig. 2(b)]. The composite is sandwiched between transparent conductive layers such as indium tin oxide (ITO). The liquid crystals are birefringent (i.e., having two different refractive indices) materials—their refractive indexes are different at different orientations of liquid crystals. For instance, MLC-9200-100—a commercial liquid crystal—has a refractive index of $n_e = 1.49$ (at the ordinary orientation of the crystals) and $n_o = 1.61$ (at the random orientation of the crystals) at 550 nm light.[93] The polymeric matrix with the refractive index that matches that of the liquid crystal's ordinary refractive index is used to develop PDLC. In the absence of an electric field (i.e., off-state), the liquid crystals are randomly orientated. Hence, PDLC at the off-state appears hazy and milky by light scattering across the inhomogeneous optical medium of random orientated refractive index. On the other hand, in the on-stage (i.e., in the presence of an electric field), the liquid crystals are reoriented such that the ordinary direction aligns parallel to the field. Hence, the refractive index is matched which leads to specular transmission and the material appears transparent. With a relatively cheaper price and availability in the sheet form that can be bonded to existing window panels, such types of switchable devices have gained popularity. However, their moderate transmittance tuning capability (~60%) and short life upon heat and UV light exposure are the major limitations that need to be addressed.

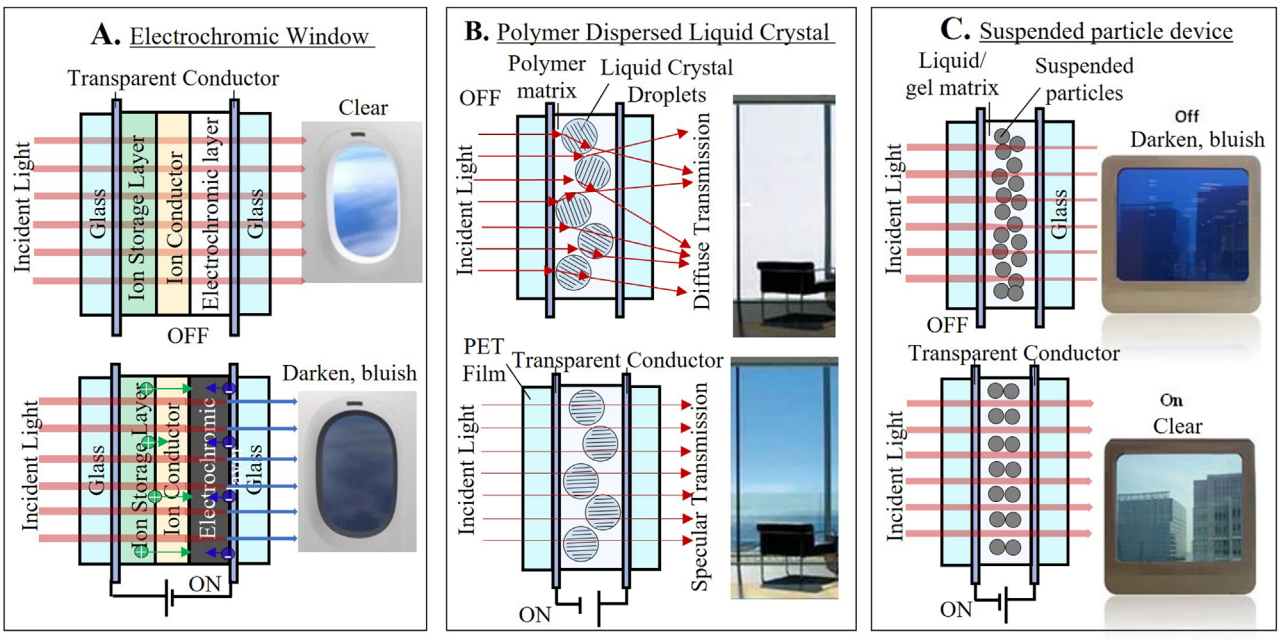

FIG. 2. Types of commercially available tunable window technologies: (a) electrochromic glass: (upper) at transparent stated; (lower) at tinted state; (b) polymer dispersed liquid crystals glass: (upper) at inactive light-diffusing state; (lower) at active and specularly light-transmitting state; (c) suspended particle device: (upper) at inactive tinted state; (lower) at active transparent state.

Transmittance tunable windows based on suspended particle devices (SPD) have found a niche commercial market.[88,94,95] SPD is known for tuning the quantity of light absorption in the presence of an electric field. SPD is also a multi-material system, which comprises needle-shaped particles well dispersed in a gel matrix or organic liquids [Fig. 2(c)].[96,97] Paraphathite or polyiodide particles (~1 μm long)[84] are usually used in SPD. Likewise, the SPD is also sandwiched between transparent and conductive layers. In the absence of an electric field, the suspended particles are haphazardly orientated and, thus, absorb the light to appear cloudy or opaque. At the on-state, the suspended particles are aligned and, thus, transmit light to be transparent.[50,84] Unlike PDLC, these devices can block solar radiation and cause 55%–60% change in optical transmittance.

Table I shows a comparison of the conventional devices in terms of transmittance tuning performance and cost. The commercial devices are still expensive; prone to fast aging upon UV exposure or have limited transmittance tuning range. Electrochromic glasses have improved in performance over recent years, yet providing complete visual privacy is still a challenge for this technology. In addition, they tend to age fast under UV exposure. Meanwhile, due to the hazy nature of PDLC, attaining a completely transparent state is a challenge. However, easy installation as a window laminating layer and the relatively cheaper cost is making them more popular in offices and commercial buildings. SPD has been seen so far in niche high-end markets like aviation. The acceptance in the wide market is still hindered by cost and availability. Several new technologies that are potentially alternative to the conventional tunable windows devices are comprehensively reviewed in Sec. III.

III. EMERGING TECHNOLOGIES FOR ACTIVELY TUNABLE WINDOWS

Recently, a swift emergence of new technologies for actively tunable windows can be witnessed. To be considered as an alternative to commercially available technologies, the emerging technologies mostly concentrate on areas such as energy and cost-efficiency, facile fabrication/development methods, controlled mechanisms, use of readily available materials, prolonged operational life, and better optical transmittance modulation range and fast response. Classifying these actively tunable windows based on optical principles offers a deeper understanding of such devices. Understanding the basic principle of operation helps interested researchers and engineers to optimize the performance and trigger new ideas to improve them or integrate additional functionalities. Here, the emerging technologies are classified into three types based on the mode of alteration/tuning of light transmitting through the devices. First, absorbance tuning; second, reflectance tuning; and third diffuse transmission. The latter—diffuse transmission—can be achieved via different methods such as particle scattering and surface scattering; hence, it is sub-classified accordingly (Sec. III C).

A. Tunable light absorption

Tunable window devices can tune their transmittance by adjusting their optical absorbance—for instance, electrochromic glass can absorb light by changing color from light to dark in the presence of an electric field.[54–56] The transmitted light (I) through an optical absorbent medium is defined according to the Beer–Lamber law,[100,101]

$$I = I_o e^{-\mu t}, \tag{2}$$

where I_o is the incident light intensity, μ is the linear attenuation coefficient, and t is the optical thickness of the absorbent medium. μ can be changed with the depth of color, for example, the redox reaction in electrochromic glass bleaches their color (i.e., altering its μ).

The dye-filled transparent polymers are known for absorbing light.[102] The light absorption of such polymers improves with the increasing dye concentration. At the given concentration of dye, the surface concentration can be decreased by thinning (reducing the thickness) of the dye-filled polymer. This offers a mechanical method to tune the optical absorbance and transmittance of the dye-filled transparent polymer [Fig. 3(A-g)]. For example, López Jiménez *et al.*[102] developed dye-suspended polymer composites to make a transmittance tunable device. In such dye-suspended polymers, the micrometer-sized dye particles are homogenously distributed in a transparent matrix (e.g., polydimethylsiloxane, PDMS). The light absorbance of such polymers is associated with the spatial density of the dye particles [$A = \log(e^{\mu t}$, where A is the light absorbance and μ and t are the same as defined in Eq. (2)]. Tuning the light absorbance

TABLE I. Comparison of the performance (transmittance, response time, and power requirement) of the conventional tunable window devices.

Window device	Substrate	Transmittance change at 550 nm	Response time	Power	Sale price (brand) as in 2016	Remarks on pros and cons	Ref.
Electro-chromic	Glass	5%–65%	300 s (5×20 cm^2)	0.1–0.5 W h/m^2	\$500–1000/m^2	Can adjust solar radiation transmission; rigid, costly, fast aging	50, 76, 86
PDLC	Polymer composite	6%–62%	500 ms	5–20 W/m^2	\$100–400/m^2	Cheaper; available in sheet form; Hazy even at ON state; no use for heat regulation	50, 72
SPD	Glass	2.4%–59%	100–200 ms	1.9–16 W/m^2	...	Can adjust solar radiation transmission; low transmittance tuning range; not well commercialized	50, 98, 99

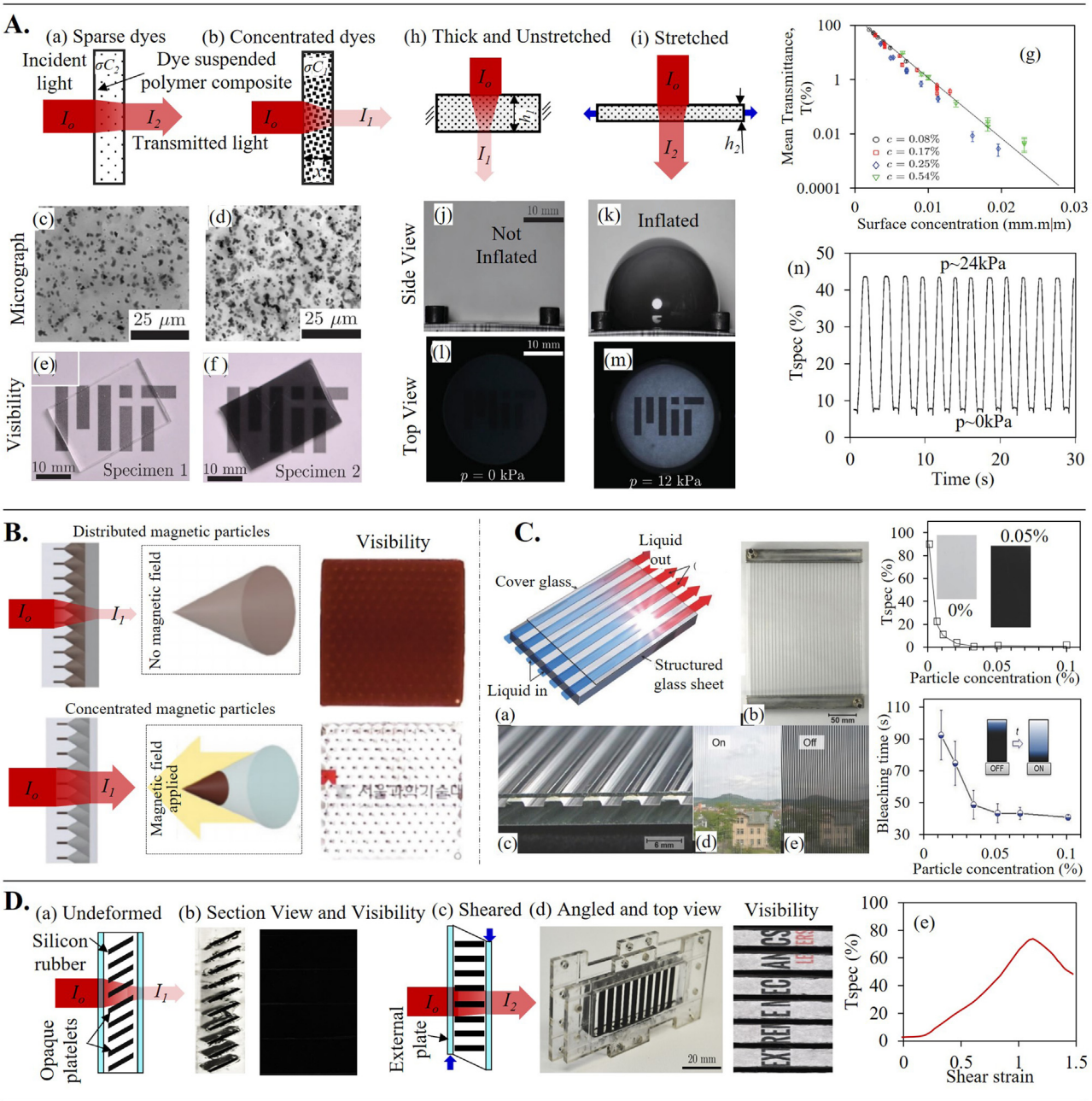

FIG. 3. Tunable light-absorbing devices based on the Beer–Lambert law: (A) Variation of the opaque particle concentration for transmittance tuning: [(a) and (b)] schematic of light transmission through the polymer with lower and higher particle concentrations; [(c) and (d)] optical micrograph of the same polymers; [(e) and (f)] visibility through the polymer having low and high dye concentrations; (g) transmittance change vs surface concentration of the dye. Mechanically stretching dye suspended polymers to reduce surface particle concentration: (h) unstretched state; (i) stretched too thin down; [(j)–(m)] the change in visibility attained by inflating the polymer composite balloon; (n) the transmittance plotted against the cyclic loading–unloading [Reproduced with permission from López Jiménez *et al.*, Adv. Opt. Mater. **4,** 620 (2016). Copyright 2016 John Wiley and Sons, Inc.].[102] (B) Controlled dispersion of magnetic nano-pigments in a pyramidal array: schematic of light transmission and visibility through the pyramidal array with homogeneously distributed nano-pigments and the same when pigments are concentrated at the pyramid tips using a magnetic field [Reproduced with permission from Yang *et al.*, Adv. Mater. Technol. **4**, 1900140 (2019). Copyright 2019 John Wiley and Sons, Inc.].[103] (C) Controlled concentration of magneto-active liquid in a microchannel array: [(a)–(c)] schematic, real prototype front, and isometric view; [(d) and (e)] visibility at on and off states presenting the uncharged and charged fluid; transparency and response time dependence on the magneto-active fluid's concentration [Reproduced with permission from Heiz *et al.*, Adv. Sustainable Syst. **2**, 1700140 (2018). Copyright 2018 John Wiley and Sons, Inc.].[104] (D) Rotation of opaque platelets embedded in silicone elastomer by shear loading. Schematic, real device, and visibility though the device: [(a) and (b)] in the undeformed state; [(c) and (d)] at sheared state; and (e) tuning transparency by shear strain [Reproduced with permission from Jiménez *et al.*, Extreme Mech. Lett. **9**, 297 (2016). Copyright 2016 Elsevier Ltd.].[105]

is tuned by stretch-induced thinning (change in thickness) of the dye-filled polymer [Figs. 3(A-h) and 3(A-i)].[102] Like blowing a balloon, the dye-filled polymeric layer can be thinned by inflating and bulging [Figs. 3(A-j)–3(A-m)]. For instance, such a method of actuation showed a change in transmittance from 5% (at 0 kPa) to 45% (at 24 kPa) and the change in transmittance is highly repeatable in the cyclic loading (inflation and deflation) [Fig. 3(A-n)].[102] However, a disadvantage of such systems is the requirement of the strain for such a transmittance change—which is usually above 100%. The requirement of such a large strain makes these devices impractical for real application (Table II).

Likewise, the liquid suspensions with light-absorbing dyes are able to attain various light absorbances depending on the particle concentration [Figs. 3(A-a) and 3(A-b)]. For dye-filled suspensions, the linear attenuation coefficient (μ) is given as $\mu = \sigma C$, where σ is the cross section area of the dye and C is the concentration of the dye. As illustrated in Figs. 3(B) and 3(C), magneto-active particles filled suspension can be adjusted to vary their particle concentrations.[103,104,106] Magneto-active particles respond to an external magnetic field to move particles as designed. Such motion is used to control particles' concentration and eventually light absorption.[103,104,107–109] For example, Yang *et al.*[103] developed switchable windows where switching between light-absorbing and not absorbing states was achieved by the movement of magnetic nanoparticles (Fe_3O_4) in the presence of a magnetic field [Fig. 3(B)]. The magnetic particles were distributed asymmetrically, thus, the magnetic particles could be moved in the presence of a magnetic field. Furthermore, the light absorption was enhanced by matching the refractive index of the matrix and the magnetic particles. In a recent study, Seo *et al.*[108] also manipulated the light transmission by taking the advantage of the alignment of the magnetic chains—the light transmission is higher when the light is illuminated parallel to the magnetic chains and is blocked when light is illuminated perpendicular to the magnetic chains. A few other studies where magnetic particles are used to manipulate light include.[104,107,109]

The surface concentration of light-absorbing particles can also be altered by using micro-blinds. Figure 3(D) shows a transparent polymeric matrix filled with parallel light-absorbing polymer micro-blinds. Jiménez *et al.*[105] used a shear strain on the polymer matrix to cause such soft micro-blinds to open or close. These devices cause the change in optical transmission like real window blinds but on a microscale so that they are not easily perceivable to naked eyes. The only drawback of this technique is the poor scalability and low efficiency of the real window size devices.

B. Tunable light reflection

Modulation of the reflected beam can be used to adjust transmittance and daylight through a window. A perfect mirror can reflect all incident light rays preventing light transmission. Reflection of light through a glass/metal interface follows Fresnel equations, where metal's dielectric function and refractive index are complex-valued functions.[101,110,111] Alteration of the interface metal's optical properties via chemical changes can modulate light reflection through the interface. A conventional mirror is made up of transparent glass, a highly reflective coating (e.g., shiny metal such as silver), and an opaque back-coat (e.g., dark paint). In contrast, there are also switchable mirrors, which are capable of switching from a reflective state to a transparent state and vice versa—through the transition of metals to the metal hydrides.[112–117] However, it should be noted that the requirement for chemical changes hinders their large-scale commercial applications.

Recently, new types of switchable mirrors have been developed to switch between total reflection and transmission (refraction) across two optical and dielectric mediums. Such devices work based on opto-mechanical (i.e., mechanical tuning transmittance) and opto-fluidic (i.e., using fluid to tune transmittance) variation. They utilize mechanically alterable shiny surfaces[118–120] or fluid-induced total internal reflection to make switchable glasses.[57] For the light traveling from one medium [refractive index (n_1)] to another medium [refractive index (n_2)], the normal reflectance (R) as can be obtained using the following equation [Fig. 1(b)]:[121,122]

$$R = \frac{(n_2 - n_1)^2}{(n_2 + n_1)^2}. \tag{3}$$

The incident light (at the given angle of the incident) is partly transmitted with the angle of refraction and partly reflected as per the Fresnel equations. The amount of reflected light depends mostly on the reflectance of the surface. Some MEMS (micro-electromechanical system) based panels were demonstrated in the past to obtain such switching of the surface.[118–120] Xiao *et al.*[87] and Mori *et al.*[89] separately demonstrated devices consisting of an array of micro-blinds or micro-shutters capable of switching from transparent to reflective upon

TABLE II. Comparison of the tunable window devices based on tunable light absorption.

S. no.	Type	Method of transmittance tuning	Substrate/light absorber	Total thickness (t)	T_{spec} at 550 nm	Reference
1.	Dye-filled transparent polymers composite	Stretch induced the thinning of substrate	PDMS/black dye (silc-pig, smooth-on)	1.5–2.5 mm	5%–45%	102
2.	Magneto-active particles filled suspension (cone-shaped chambers)	External magnetic field to control the concentration	Molded PDMS/(Fe_2O_3 nanoparticles in IPA/PEG solution)	3.5 mm	30%–80%	103
3.	Magneto-active particles filled suspension (parallel channels)	External magnetic field to control concentration	Glass/suspension of Fe_3O_4 nanoparticles in monopropylene glycol	4–6 mm	0%–90%	104
4.	Microblinds embedded in a transparent polymer	Shear strain-induced rotation of microblinds	PDMS/opaque platelets (silc-pig, smooth-on)	20 mm	0%–75%	105

voltage activation [Fig. 4(A-c)]. The micro-blinds are made of metal-laminate, such as SiO_2 microcantilever, which can be rolled by default due to the unimorph effect of the cantilever. At the off-state, the rolled microcantilevers allow the open micro-apertures to transmit light [Fig. 4(A-d)]. Voltage activation unrolls the micro-cantilevers using electro-static force and reduces the micro-apertures. When the micro-apertures are completely covered by the reflective micro-cantilevers, the panel appears reflective concealing the view [Fig. 4(A-e)]. These devices need voltage up to 55 V to change the mechanical aperture from 0% to 55%—which corresponds to a change in optical transmittance to 53% from 36%.[118–120] Despite being fast and reliable, these devices use complicated fabrication techniques and can be very expensive.

Unlike the microshutter-based devices, the optofluidic device uses total internal reflection to adjust optical transmittance. Total internal reflection occurs only if the incident angle of the light rays is greater (or at least equal) than the critical angle (θ_c), and θ_c can be obtained using the following equation:

$$\theta_c = \arcsin\left(\frac{n_1}{n_2}\right). \quad (4)$$

When the total reflection criterion is met, all the incident light will be reflected and this phenomenon is known as the total internal reflection [Fig. 4(B-c)]. For this phenomenon to happen, the incident light must be traveling from the higher refractive index (n_2) medium to the lower index (n_1) medium. For instance, a diver could observe the illusion of fish in the air caused by the total internal reflection of a fish under the water. Total internal reflection can be utilized to switch from transparent to opaque. For example, Wolfe and Goossen[57] reported optofluidic smart glass utilizing this phenomenon to make switchable windows. These switchable optofluidic glasses are made up of an array of corner cube reflectors with transparent material—vero clear (from Stratasys, Ltd., $n = 1.52$ at $\lambda = 589$ nm) was used as a transparent material [Fig. 4(B)].[57] The corner cubes were designed at angled more than the critical angle (i.e., $\theta_c = 41.1°$)—hence, incident light (normal to the device) will be traveling via multiple total internal reflections. As a result, the device appears opaque. However, if the compartments are filled with fluids having a matching refractive index with vero clear, the light would simply refract through it. When methyl salicylate was used as a filling fluid, the transmittance was tuned from 85% to 8% in their study.[57] However, such devices need a pump to fill the liquid for active operation—therefore creating sealing and safety issues.

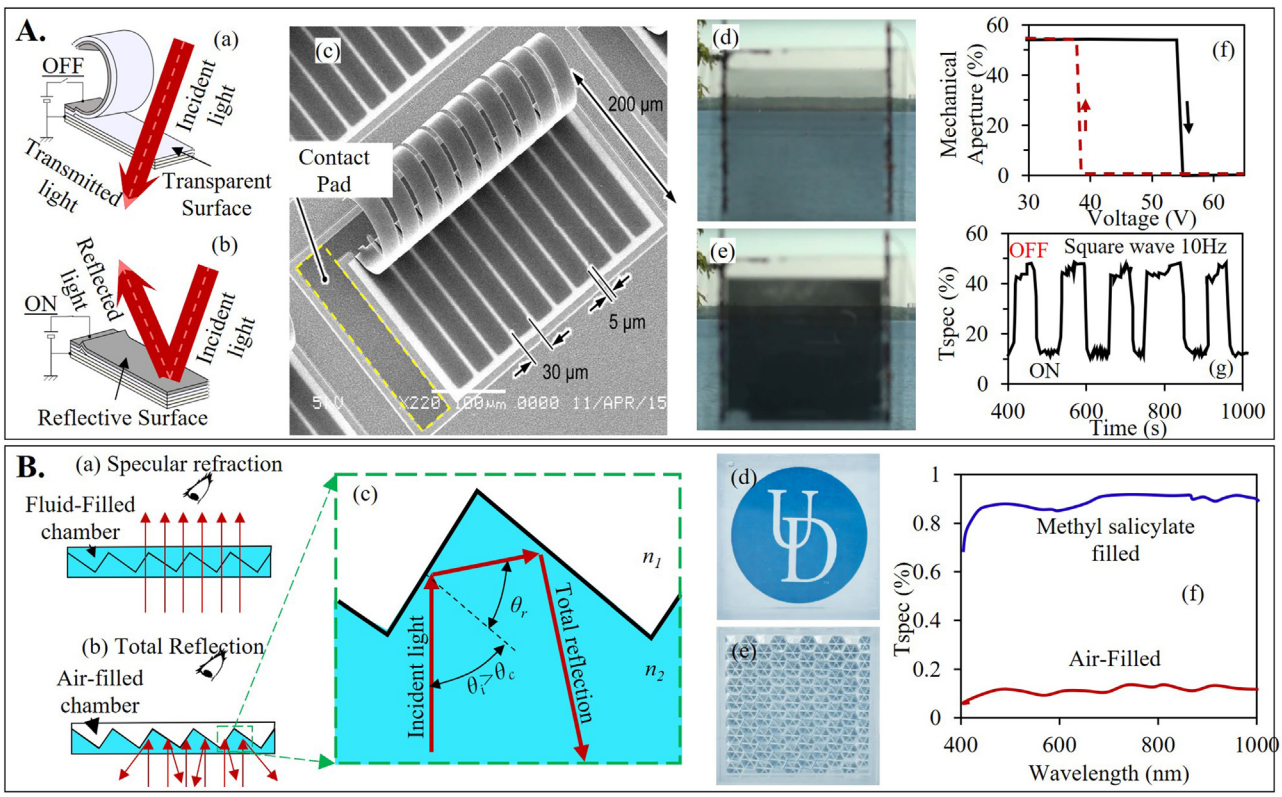

FIG. 4. Switchable windows based on tunable light reflection. (A) Tuning light reflection by adaptable micro-shutters: (a) schematic of light transmission when the micro shutters are open; (b) reflection of light when micro-shutters are closed; (c) SEM image of the micro-shutters; (d) visibility through the device when micro-shutters are open; (e) when micro shutters are closed; (f) change in aperture upon voltage activation of the micro-shutters; and (g) change in transmittance upon cyclic activation of the device [Reproduced with permission from Mori *et al.*, IEEE Photonics Technol. Lett. **28**, 593 (2016). Copyright 2016 IEEE].[120] (B) Total internal reflection-based optofluidic smart glass: (a) schematic of the transmission through the fluid-filled chambers with matching refractive index; (b) the total reflection of the empty chambers; (c) amplified graphic of total internal reflection; (d) visibility through the device when filled with fluid; (e) visibility when chambers are empty; and (f) transmittance of the fluid-filled chamber based device at empty and fully filled conditions [Reproduced with permission from Wolfe *et al.*, Opt. Express **26**, 2 (2018). Copyright 2018 Optical Society of America].[57]

C. Tunable light transmission

The beam of light-transmitting in a medium can be scattered by optical diffusers.[123] For example, optically clear polymers or substrates can be hazy if the optical scatterer or diffusive materials are loaded into them. This variation of the transmitting light can be used to make tunable glasses that are suitable for the visual privacy preservation of indoors. There are two types of optical scattering, namely (1) scattering by particles and (2) scattering by micro-rough surface (Fig. 5). First, particle scatterers include micro-defects or micro-droplets (of different refractive index) or transparent particles, loaded into transparent polymer matrices. For example, even air voids in a clear polymer matrix can diffuse light by spatial inhomogeneity of refractive index. Light scattering by particles works based on Mie scattering.[123] Second, the micro-rough surfaces in the transparent medium trigger the random spatial distribution of the incident light and then help to diffuse the light.[122,124,125] To actively adjust the optical diffusion, tunable window devices can vary the micro-geometry to scatter the light, which is inherently clear.

1. Particle or Mie-scattering

The theory of light scattering by particles hugely depends on the size of the scattering particles. Rayleigh scattering is defined as the elastic scattering of light—which occurs within uniform particles with a diameter smaller than that of the incident light wavelength [Fig. 5(A-b)].[123,126] For example, the sky appears blue as the air molecules can strongly scatter the short-wavelength blue and violet lights than they can scatter the longer wavelength yellow or red lights.[71] Mie scattering, on the other hand, is caused by particles with a diameter similar to or larger than that of the incident light wavelength [Fig. 5(A-c)].[127] The appearance of cloud and fog (i.e., white usually) is a result of Mie scattering by various microscopic particles in the air such as dust, pollen, and smoke or even water droplets. Mathematically, in the Mie scattering regime, the scattered intensity is inversely proportional to the square of the wavelength of the incident light—while Rayleigh scattering is inversely proportional to the fourth power of wavelength.[71,126,127] Consequently, Rayleigh scattering is always weaker than Mie scattering. Hence, Rayleigh scattering is more applicable to mechano-chromic (i.e., mechanically obtaining various colors) devices to change colors,[128,129] while devices using Mie scattering are could be used to tune haziness of the windows. This article mostly reviews devices using Mie-scattering to abide the scope of this article.

Inhomogeneous distribution of the refractive index can be introduced to a transparent polymeric matrix by loading submicrometer particles of transparent materials.[130,132] The inhomogeneity introduced by filler particles makes the composite (i.e., matrix filler system) hazy via Mie scattering when the light is illuminated. On the other hand, to achieve clarity, the blend must make use of submicrometer filler materials whose refractive index is matched with the transparent matrix.[132,134] For a passive matrix-filler system, the haziness or clarity is permanent once it is fully polymerized. However, haziness can be tuned by manipulating the optical scatters through mechanical and/or thermal stimulations. In the presence of such external stimuli, the following phenomena could occur. First, the haziness can be tuned by varying the surface particle density, similar to how visibility is different for different fog densities.[135,136] Second, mechanical stretch induces the generation and collapsing of air voids/bubbles within the polymer matrix acting like optical scatterers.[131] Third, mechanical stretch induces a change in the orientation of liquid crystals embedded in the polymer matrix.[131] Fourth, the haziness can be tuned by changing the phase of particles by melting and solidification.[134] Fifth, the formation and collapsing of micro-crystal boundary in a crystalline panel also can tune the haziness.[131]

a. Variation of surface particle density. Highly adjustable hexagonal diffraction grating was developed using polystyrene (PS) particles (1 μm in diameter, n = 1.58 at λ = 550 nm[137]) on a plasma-treated PDMS film.[130] The PS particles were tightly packed forming a hexagonal ball-grid-like array on the PDMS film [Fig. 6(A)]. Such an array of PS particles diffracted the laser beam into a hexagonal pattern—it contains a primary center spot and six secondary spots near the vertices of the hexagon. When the PDMS is stretched the distance between PS particles will be changed—while the total transmittance of the device is maintained high and not dependent on the stretch ratio, but the specular transmittance slightly depends on the stretch ratio. They reported a change in specular transmittance to 26% from 19% at 75% stretch.[130]

b. Variable void formation. Forming and collapsing voids in a polymer matrix can provide a means to manipulate the Mie-scattering of light through the polymer.[129,131,132] Ge *et al.*[131] used silicone rubber and silica nanoparticle composite—silicone rubber matrix (n = 1.42 at λ = 632.8 nm) and silica nanoparticles (n = 1.45 at λ = 632.8 nm)—to produce a transparent film with uniformly distributed refractive index. When such a composite is exposed to the mechanical stretch, the delamination between elastomeric matrix and silica nanoparticles induced air voids formation. The air void volume V_{void} was projected to be linearly varying with the amount of the strain ε as $V_{void} = \varepsilon V_{silica}$, where V_{silica} is vol. % of silica loading.[131] Figure 6(B) depicts the normal transmittance vs strain of the device. It was found that the strain-induced rate of transmittance reduction was also slightly dependent on the size of the silica nanoparticles—PDMS with 306 nm silica nanoparticles showed a gradual reduction of transmittance compared to 221 nm silica nanoparticles.

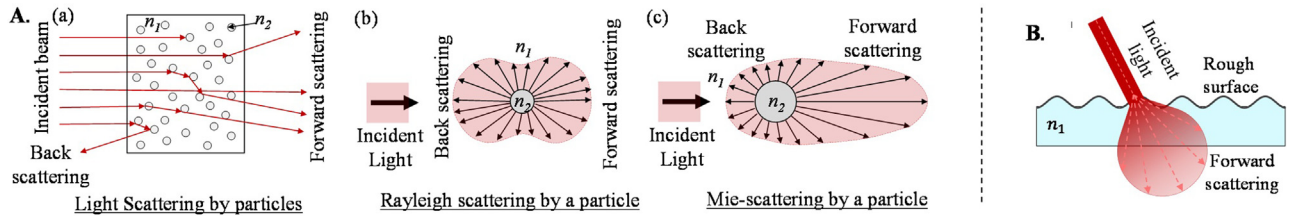

FIG. 5. Illustrations of various methods for the forward scattering of the light. (A) Light scattering by particles: (a) schematic of multiple light scattering by scattering particles loaded transparent matrix; type of light scattering based on particle size, (b) Rayleigh scattering by small particles (relative to the wavelength of light), and (c) Mie scattering by larger particles (relative to the wavelength of light). (B) Light scattering by the micro-rough surface.

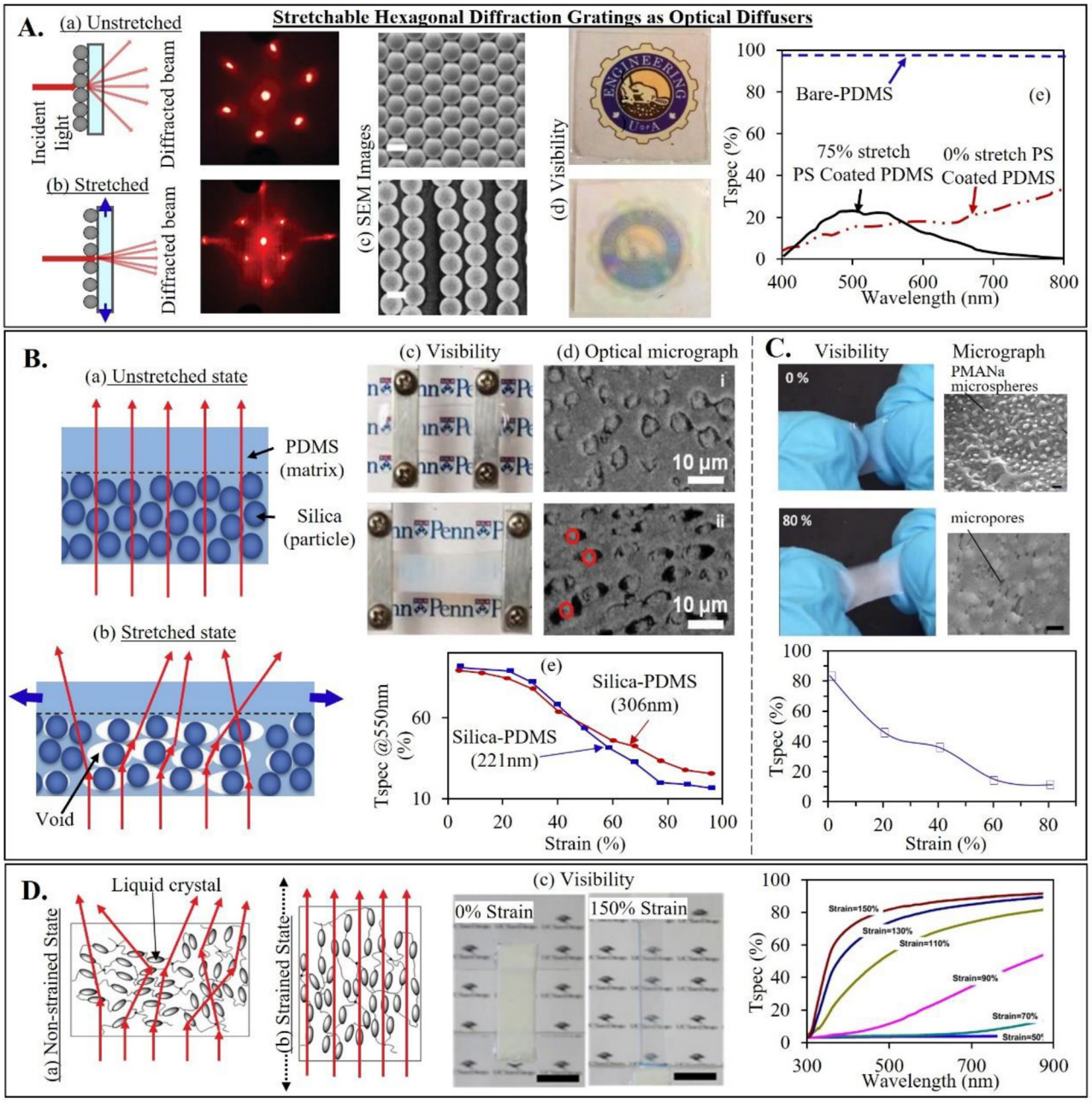

FIG. 6. Transmittance tuning of devices that alters Mie-scattering through mechanical stretching. (A) Stretching of a tunable optical diffuser made up of PDMS layer with polystyrene (PS) microspheres assembled on its surface: graphical illustrations, microscopic images, and light diffraction patterns: (a) at passive state, (b) 75% stretching; and (c) corresponding change in transmittance achieved from the devices [Reproduced with permission from Mahpeykar *et al.*, Adv. Opt. Mater. **4**, 1106 (2016). Copyright 2016 John Wiley and Sons, Inc.].[130] (B) Forming voids in the silica nanoparticle-PDMS composite by the mechanical strain to scatter light: [(a) and (b)] illustration of unstretched and stretched composite; (first and second rows): (c) optical micrograph and (d) visibility through the composite membrane-unstretched and stretched by 100%; (d) change in transmittance via straining the composite film [Reproduced with permission from Ge *et al.*, Adv. Mater. **27**, 2489 (2015). Copyright 2015 John Wiley and Sons, Inc.].[131] (C) PMANa/polyurethane (PU) membrane with naturally occurring microsized spheres and pores upon stretching: (left) visibility through the device and the SEM images of the surface at unstretched and stretched states; (right) change in transmittance upon mechanical strain [Reproduced with permission from Si *et al.*, ACS Appl. Mater. Interfaces **12**, 27607 (2020). Copyright 2020 American Chemical Society].[132] (D) Mechanical strain-induced alignment of mesogen in the liquid crystal elastomer (LCE): (a) randomly oriented mesogen in polydomain LCE strongly scatter light; (b) stretching the LCE aligns the mesogens making it monodomain and transmit light; (c) visibility through the unstretched and stretched LCE; (d) change in optical transmittance by stretching the LCE [Reproduced with permission from Wang *et al.*, Extreme Mech. Lett. **11**, 42 (2017). Copyright 2017 Elsevier].[133]

On the other hand, transmittance reduction of PDMS with 306 nm silica nanoparticles was relatively independent of the incident light wavelength—it signified that the air voids formed within the PDMS with 306 nm silica nanoparticles were primarily via the Mie-scattering effect. In the meantime, the Rayleigh scattering must be dominant for air voids within the PDMS with 221 nm silica nanoparticles. The transmittance of the PDMS (unstretched) silica composite was as high as 90%—and 100% strain could decrease the transmittance to 20%. Si *et al.*[132] also demonstrated a similar device based on poly methacrylic acid sodium salt (PMANa)/polyurethane (PU) latex-polyelectrolyte colloids. The microspheres of PMNA were homogeneously distributed in the PU matrix and appeared transparent. Upon stretching the membrane due to the elastic modulus mismatch between the PMNA and PU, a void is formed by the detachment of the interfaces. Notably, the transmittance was tuned from 84% to 12% with 80% uniaxial stretching [Fig. 6(C)].

c. Variable liquid crystals orientation. A polydomain Liquid crystal elastomer (LCE) is opaque.[138,139] The randomly oriented liquid crystal domains are several hundreds of nanometers and can strongly scatter light. Upon mechanical stretch, the liquid crystal mesogens align becoming monodomain LCE. Such stretching can transform opaque polydomain LCE to transparent monodomain LCE.[138,139] Such mechano-optical coupling effects can be utilized to make privacy glasses. Wang *et al.*[133] demonstrated such a device capable of changing specular transmittance from 0% to approximately 75% with 150% uniaxial stretching [Fig. 6(D)]. Other examples of recent studies on electrically tunable LC devices similar to PDLC are Refs. 140–144.

d. Phase separation by melting. A common example of this is a paraffin film—which looks hazy as it contains crystallites of long alkyl chains. However, liquid paraffin turns optically very clear as the crystallites melt and become amorphous liquid.[134,145] An elastomeric composite was developed by homogenously distributing paraffin crystals (5 μm size and 10 wt. % loadings) within a silicone-based elastomer [Fig. 7(A)].[134] At the room temperature, the paraffin crystals have a higher (by 7%) refractive index than that of PDMS elastomer—the composite also

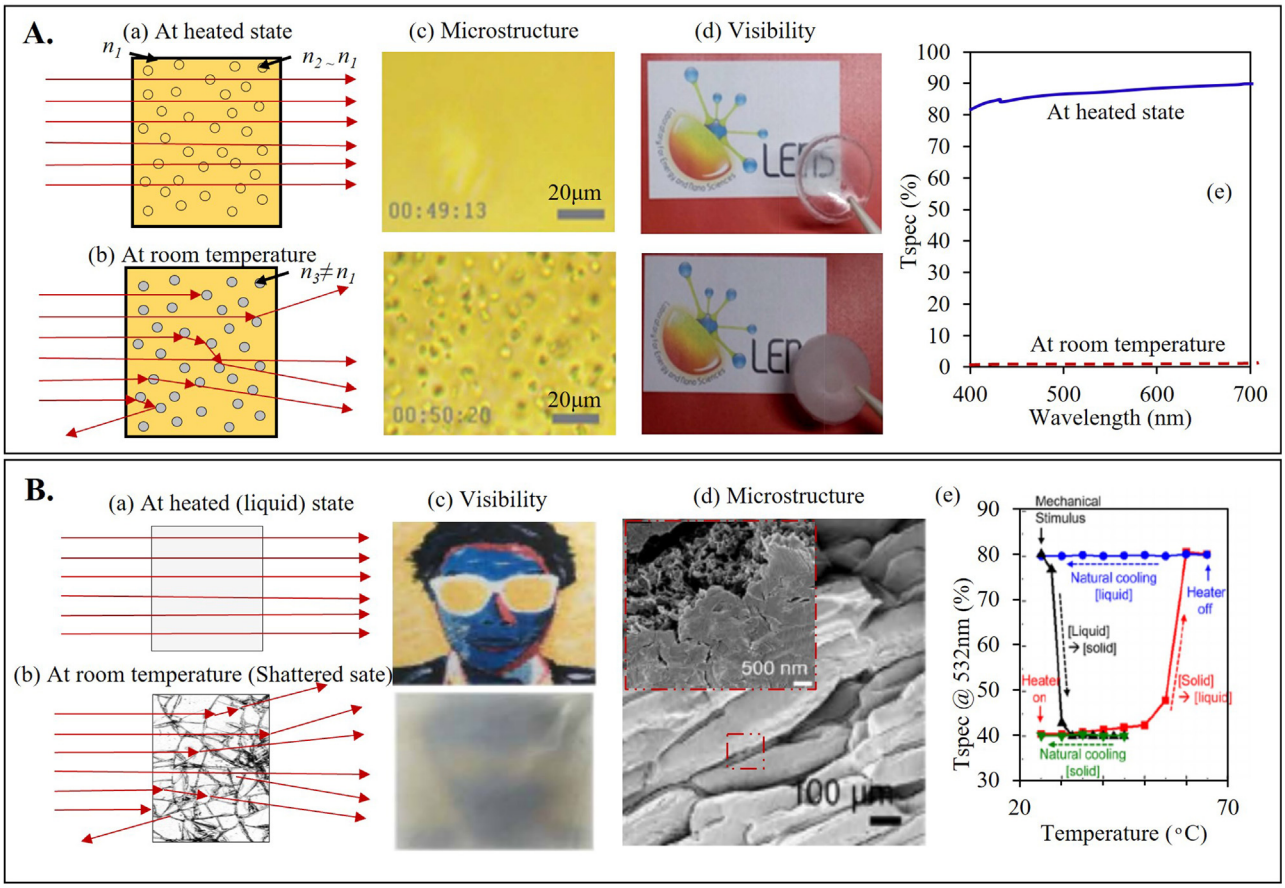

FIG. 7. Transmittance tuning by thermal stimulation of devices that uses Mie-scattering. (A) Paraffin-filled PDMS film becomes transparent at elevated temperature and appears opaque at room temperature: graphical representation of the light transmission through it (a) at elevated temperature, (b) at room temperature, (c) corresponding change in the microstructure and (d) visibility through the films, (e) transmittance plotted against light wavelength at room and elevated temperatures [Reproduced with permission from Apostoleris *et al.*, J. Mater. Chem. C **3**, 1371 (2015). Copyright 2015 Royal Society of Chemistry].[134] (B) Phase change of the supersaturated salt hydrate crystal to scatter light: graphical representation of light transmitting through the crystal at (a) heated liquid or cool-unshattered state; (b) cooled and shattered stated; (c) visibility through the crystal at the two states; (d) microstructure of the cooled and shattered crystal; (e) (NO_e in the figure) change in transmittance by heating, cooling, and mechanically shattering the crystals [Reproduced with permission from Cho *et al.*, Sci. Adv. **5**, eaav4916 (2019). Copyright 2017 AAAS].[147]

appears hazy at room temperature. At the elevated temperature (>46 °C), the composite becomes less hazy. However, the same composite film sandwiched between a PET (polyethylene terephthalate) layer and a pure PDMS layer appears hazier (only 0.5% transmittance) below the melting point of paraffin (56–58 °C). An electro-thermal activation was used to heat the composite film—graphene resistive film on PET could melt paraffin when activated by 18 V and 0.33 W/cm^2 and, hence, the transmittance was increased to 85%.[146]

e. Formation of the micro-crystal boundary. A solid panel made of the transparent polycrystalline material appear hazy due to the scattering of light by the micro-crystals boundary.[148] Meanwhile, a single solid bulk of the crystal can be transparent. For instance, Cho *et al.*[147] used a supersaturated[149] sodium acetate solution, which is a transparent liquid at 60–65 °C. Upon cooling the solution forms a transparent single crystal. At both of these states, the panel made of such a solution or crystal has a transmittance of 80%. However, an intentional mechanical impact on one corner of the crystal causes the shattering of the whole crystal into numerous micro-crystals, which scatters light and the specular transmittance drops to about 40%. These crystals can be made transparent again by reheating to 65 °C [Fig. 7(B)].

2. Surface scattering (rough surfaces)

A tunable optical diffuser with variable surface roughness is another prominent category of actively tunable window technologies. This method is driven by the interesting fact that the flat glass with a smooth surface appears optically clear; however, the ground glass with a rough surface appears translucent or hazy. For in-depth understanding and optimization of these devices, an understanding of the surface scattering principle is needed. A flat glass enables the specular transmission of light, which can be refracted two times [Fig. 8(a)]. Assuming negligible light absorption by optical medium, the total transmittance across each interface follows the Fresnel equation:[121]

$$T = 1 - R = \frac{4n_1 n_2}{(n_2 + n_1)^2}, \tag{5}$$

where n_1 and n_2 are the refractive indices of two optical media at the interface. For instance, the glass refractive index $n_2 = 1.4$ and the air refractive index is $n_1 = 1$ for the air–glass interface. However, a light beam incident on a rough surface can be diffused in various directions [Figs. 8(b) and 8(c)]. On a rough surface, light rays scatter because of the height variation, which induces phase difference (due to optical path difference). Although the total transmittance through the completely transparent material (with a diffusive surface) is always constant, the specular transmittance can be decreased. This is the reason that these types of tunable windows are suitable for visual privacy preservation functionality but unsuitable for energy control.[150]

The optical scattering power of a surface depends on its roughness. All surfaces have some level of roughness, the surface can be considered optically smooth if the Rayleigh criteria $\sigma \ll \frac{\lambda}{8\cos\theta_i}$ is satisfied, where σ is the rms surface roughness, λ is the incident light wavelength, and θ_i is the incident angle.[151] The Rayleigh smooth surface can be regarded as a poor light scatterer, and the total integrated scattering (TIS) is given as $TIS \cong \left(\frac{4\pi\sigma\cos\theta_i}{\lambda}\right)^2$. The surface to be considered as roguh according to Rayleigh criteria only if the surface can induce a phase difference greater than $\frac{\pi}{2}$.[152,153]

As given by Beckman and Spizzichino,[124,125] the specular transmittance T_{spec} through the rough surface is only a portion of the total transmittance T. The specular transmittance through a transparent plate with both surfaces having σ roughness is derived as[124,154,155]

$$T_{spec} = T \cdot \exp\left\{-\left[\frac{2\pi\sigma}{\lambda}\cos\theta_i(n_1 - n_2)\right]^2\right\}. \tag{6}$$

Equation (6) implies that the increased surface roughness (relative to the incident light wavelength) can decrease the specular transmission. Though scattering angles are dependent on the pitch of the roughness, specular transmission is independent of the pitch. This insight serves as a guide for designing an application-specific tunable optical diffuser by actively changing the surface roughness of the transparent media.

Unlike glass—which has a fixed surface roughness—the soft optical media display a possibility to tune the surface roughness in the presence of external stimuli (e.g., force, electric field, heat, etc.). A quick and easy method to change the surface roughness of the soft media with a hard-coated elastomer membrane is via mechanical compression. The unfolding of such micro-wrinkled hard-coated elastomeric membrane surface can be performed by the voltage-induced area expansion as that of a dielectric elastomer actuator (DEA) or simply by mechanical stretching. The mechanical stretching method is suitable only for a free membrane substrate. On the other hand, the voltage-induced actuation is also suitable for membrane bonded to a rigid glass. The voltage-induced actuation to change the surface

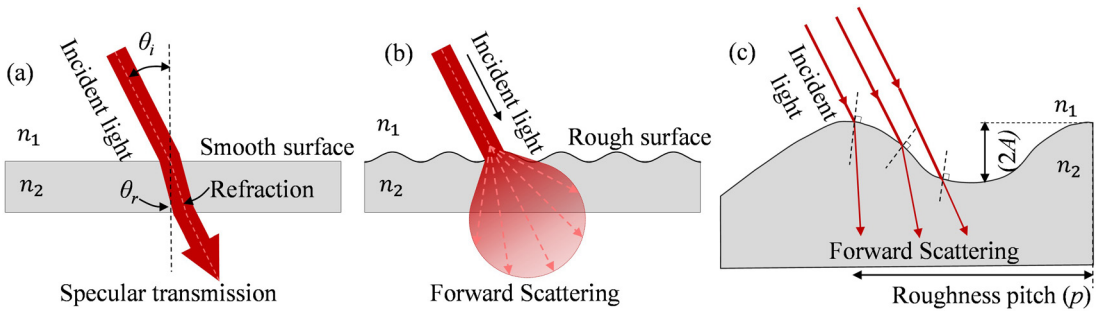

FIG. 8. Illustrations of light transmitting through various types of surfaces. (a) Specular transmission through the smooth surface (i.e., surface roughness is much smaller compared to the wavelength of light); and (b) forward scattering by the rough surface (i.e., the surface roughness is comparable to or larger than the wavelength of light). (c) A magnified view of the light being transmitted through a rough surface.

roughness works on the principle of voltage-induced surface instability or nanowire indentation of a dielectric elastomer membrane. Insights into these methods and tunable window devices developed based on these principles are described in the following.

a. Mechanically induced surface roughness. Mechanical compression can buckle a hard coating supported by a soft elastomer membrane. The compressive strain is applied by releasing the elastomer's pre-stretch.[65,156–159] This provides an easy way to change the surface roughness. However, such a device requires a large mechanical compression to affect the optical diffusion, which hinders its acceptance in real-life applications. Optimizing surface wrinkles and strain requirements need an understanding of the thin-film buckling theories. According to the plate buckling theory, the critical buckling strain follow $e_c = \frac{1}{4}\sqrt[3]{\left(\frac{3E_s}{E_f}\right)^2}$, where E_f and E_s are Young's modulus of the stiff film and soft substrate, respectively.[158] This suggests that the larger moduli mismatch (i.e., stiffer film on a softer substrate) leads to a smaller critical strain required to cause the surface buckling. As Eq. (6) suggests, the amplitude of the microwrinkles needs to be large compared to their wavelength to cause effective optical scattering. As the compressive strain increases, the surface roughness increase simply because the amplitude of microwrinkles increases. In this post-buckling scenario, the wrinkle amplitude is given by[158]

$$A = 2\pi t_f \sqrt[3]{\left(\frac{E_f}{3E_s}\right)} \frac{\sqrt{1+\nu}}{\pi} \sqrt{|e| - e_c}, \tag{7}$$

where ν is the substrate's Poisson's ratio, t_f is the thickness of surface films, and e is the compressive strain. Equation (7) is a coating film with larger stiffness (i.e., larger thickness and/or modulus) and softer substrates obtained larger wrinkle amplitude. Designing micro-wrinkled surfaces using this insight can help obtain a stronger surface scatterer even with a smaller compression strain.

Few researchers have explored the interference of light rays using tunable optical gratings made of parallel periodic surface wrinkle.[160–163] Figures 9 and 10 show such devices made of pre-stressed silicone sheets coated with glassy polymer films such as polystyrene

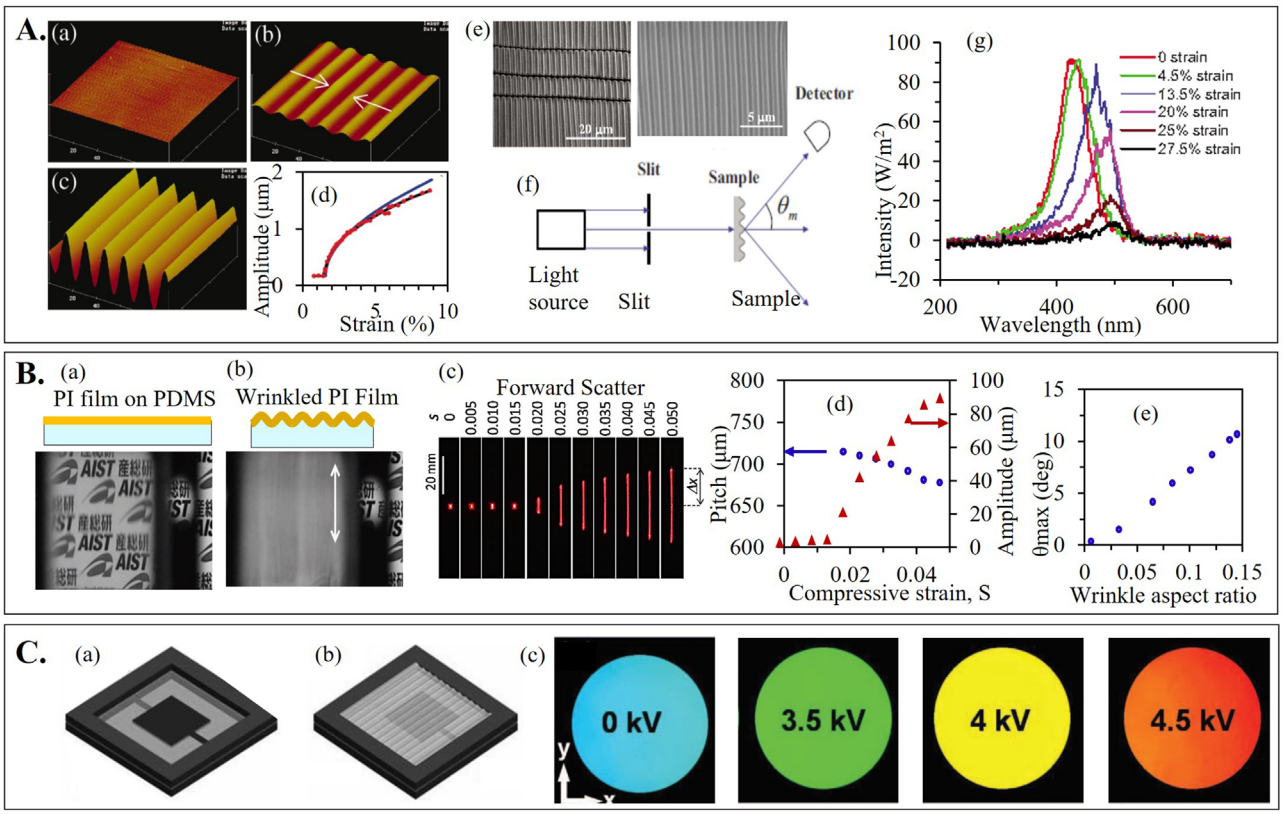

FIG. 9. Interference of light rays using tunable optical gratings made of parallel periodic surface wrinkle: (A) unidirectional light scattering by submicrometer scale diffraction grating formed of the gold/palladium film coated on PDMS: [(a) and (c)] atomic force microscopy (AFM) image of the surface at different stretched states; (d) wrinkle amplitude at various strain; € SEM image of buckling profile; (f) setup used to measure the scattering of a parallel beam of light; and (g) intensity profile of the parallel beam passing through the device [Reproduced with permission from Harrison *et al.*, Appl. Phys. Lett. **85**, 4016 (2004) and Yu *et al.*, Appl. Phys. Lett. **96**, 041111 (2010).Copyright 2010 AIP Publishing].[160,161] (B) Microwrinkling of a PDMS substrate coated with PI to scatter light. Illustration of surface and corresponding visibility through the membranes at (a) flat state; (b) wrinkled state; (c) linear diffusion pattern when a laser beam is shone through the device; (d) pitch and amplitude of wrinkles as the compressive strain progresses; and (e) corresponding scattering angle to wrinkle aspect ratio [Reproduced with permission from Ohzono *et al.*, Adv. Opt. Mater. **1**, 374 (2013). Copyright 2013 John Wiley and Sons, Inc.].[162] (C) Dielectric elastomer actuator (DEA) driven tunable diffraction grating: [(a) and (b)] schematic of off and the activated states; (c) DEA actuation to control diffracted light's wavelength as shown in images of the diffracted light [Reproduced with permission from Aschwanden *et al.*, Opt. Lett. **31**, 2610 (2006). Copyright 2006 Optica Publishing Group].[163]

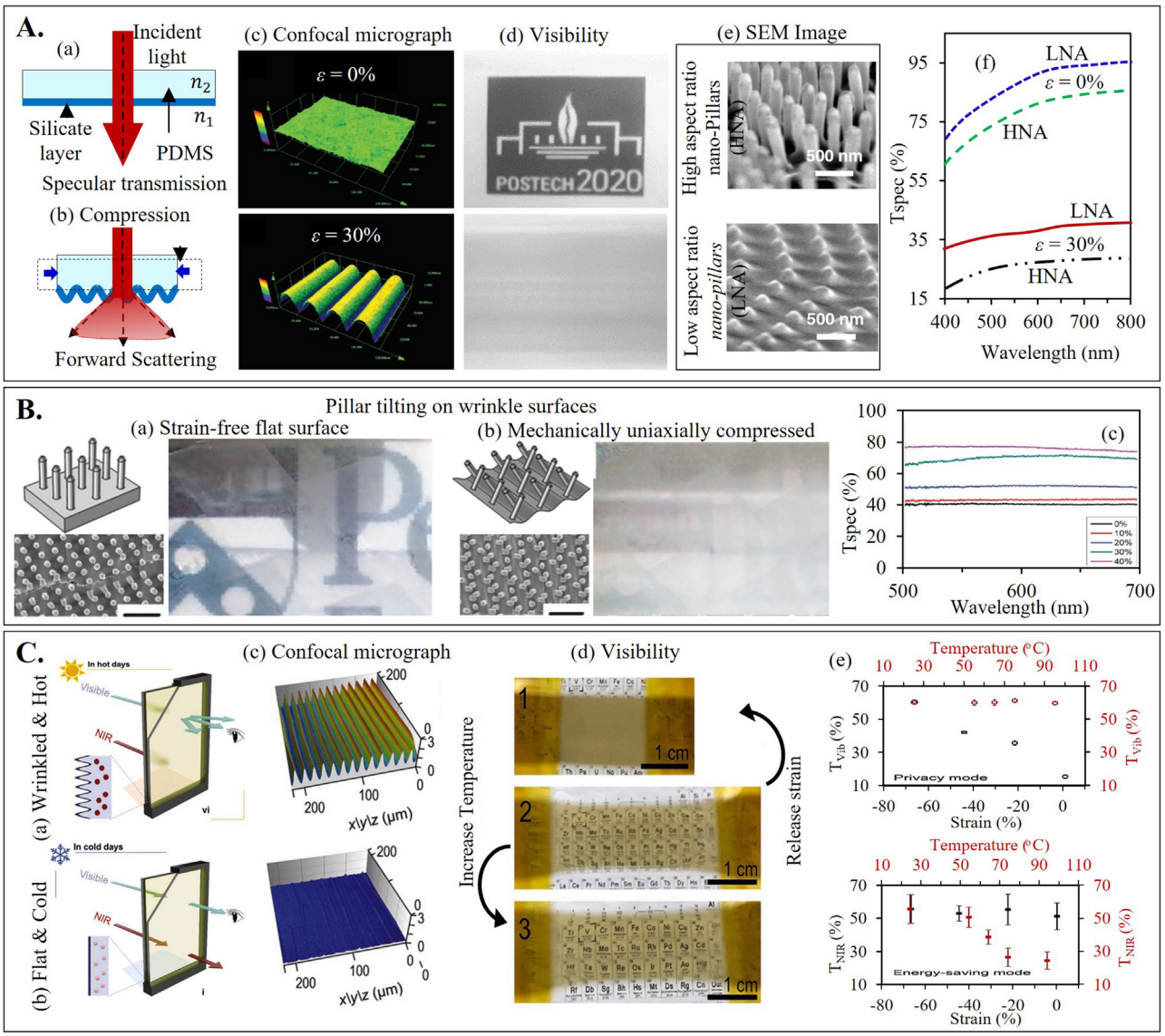

FIG. 10. (A) Deformable micro-wrinkling of a PDMS substrate with nano-pillar arrays and silicate coating to diffuse light. [(a) and (b)] Illustration of the light passing through flat and wrinkled substrates; [(c) and (d)] confocal images and visibility through the membrane at the smooth state and wrinkled states; (e) SEM images of low and high aspect ratio nanopillar arrays (LNA and HNA); and (f) specular transmittance for the same devices at 0% and 30% compression strain [Reproduced with permission from Lee *et al.*, Adv. Mater. **22**, 5013 (2010). Copyright 2010 John Wiley and Sons, Inc.].[61] (B) Switching between three states: opaque, colored, and transparent by reversibly stretching sub-micron-sized pillars on micro-wrinkles: illustrations, SEM micrographs, and visibility through the device at (a) flat state, (b) wrinkled or pillar tilted states, and (c) change in transmittance with strain [Reproduced with permission from Lee *et al.*, Adv. Mater. **26**, 4127 (2014). Copyright 2014 John Wiley and Sons, Inc.].[164] (C) Tunable light scattering of visible light by micro-wrinkling polyvinyl alcohol (PVA) coated PDMS and tunable near-infrared (NIR) light absorption by heat-induced phase change of the embedded VO_2 particles: [(a) and (b)] schematic at mechanically wrinkled-hot state when visible light is scattered and NIR is absorbed and same at flat-cold state where both NIR and visible light are transmitted; (c) confocal micrograph at wrinkled and flat state; influence of temperature and mechanical strain on (d) visibility and (e) transmittance of visible and NIR light [Reproduced with permission from Ke *et al.*, Nano Energy **73**, 104785 (2020). Copyright 2020 Elsevier].[150]

and polyimide films.[160–162] Compression of the sheets results in a sinusoidally wrinkled surface where the degree of compression and film thickness controls the wrinkle wavelength. Hence, as shown in Fig. 9(A-g), the compressive strain can manipulate the scattering angle and the color of light that pass through it. Uniaxial compression of the membranes buckles the PI films into the submillimeter-sized wrinkled surface and consequently forward diffuses the light. This makes the membranes appear hazy and conceals the behind view [Fig. 9(B-b)]. The device under 5% uniaxial compressive strain formed unidirectional wrinkles with ∼680 μm pitch and ∼88 μm amplitude [Fig. 9(B-c)]. Consequently, the device diverges the light with a maximum angle of $\theta_{max} = 12°$. In another study, Aschwanden and Stemmer[163] used

dielectric elastomer actuators (DEA) to electrically manipulate the uniaxial wrinkle's pitch which acted as a tunable diffraction grating [Fig. 9(C)]. Although the device was only able to tune the diffracted light from blue to red with an activation voltage of 4.5 kV—it shows the potential that the DEA could be used to make tunable chromic devices and windows.

Some studies have focused on tunable diffuser devices that use PDMS substrate with a hard silicate coating enabling it to form tunable surface wrinkles.[61,165] They focused on enhancing the transmittance modulation range and optical bandwidth of such devices. Lee *et al.*[61] and Lee *et al.*[164] considered the addition of nano-pillars on the PDMS surfaces to reduce reflectance and enhance optical transmittance. The pre-stretched PDMS is plasma treatment to form a hard silicate surface [Figs. 10(A) and 10(B)].[61,164] The hard silicate layer forms wrinkles as the device's pre-stretch is released. The nano-pillars were molded on the PDMS membrane prior to pre-stretching. Various aspect ratios of the nanopillars interacted differently with the incident light. The surface reflectance was reduced by low aspect ratio (LNA) nano-pillars' devices with 150 nm high pillars increasing the transmittance of the device to ~90%. On the other hand, the high aspect ratio (HNA) nano-pillars' devices with 700 nm pillars lowered the transmittance due to increased optical scattering [Figs. 10(A-g) and 10(A-h)]. A 30% uniaxial compression of LNA devices formed unidirectional wrinkles with a pitch of 31 and 4.4 μm amplitude. Consequently, it diffused the incident light and lowered its transmittance to 40%. Ke *et al.*[150] combined optical scattering using uniaxial wrinkling of PVA coated PDMS and temperature-dependent near-infrared (NIR) absorbance of vanadium dioxide (VO_2) nanoparticles to create a multifunctional tunable window. The VO_2 nanoparticles were embedded in the PDMS substrate itself and blocked NIR radiation as the temperature increased [Fig. 10(C-e)]. Meanwhile, optical scattering in the visible range was controlled by strain-induced wrinkling. Such concepts opened new pathways and multifunctionality to the non-conventional tunable windows which are discussed in detail elsewhere.[142,166–168]

Various transparent coating materials are applicable to make micro-wrinkling tunable windows. They include thin films made of polyimide,[162] graphene oxide (GO),[62] silicate,[61] and so on. The substrate materials include silicone rubber (e.g., PDMS), acrylate dielectric elastomer, and so on.[61,62,164] To make an electroactive window device (in the form of a soft capacitor), the transparent coating layers must be conductive and capable of forming microwrinkles to make compliant electrodes. As such, suitable transparent conductive materials are metallic nanometric films, mono/multi-layer graphene, transparent conductive oxides such as indium tin oxide (ITO) and other transparent conductive polymers.[64–66,169]

Figure 11 shows similar tunable diffusive devices but they used biaxially wrinkled surfaces. Figure 11(a) shows a biaxially pre-stretched 3M VHB 4910 membrane coated with a gold thin-film.[63] At the flat state, this device with 13 nm thick gold film is nearly transparent (with a transmittance of 55%). As the biaxial pre-stretch of the membrane is released, it buckles the surface of the membrane including the gold film to form ridges [Fig. 11(A-a)]. As such at a 70% biaxially compressed state, ridges of 2–4 μm amplitude and 8 μm pitch are formed. Consequently, it becomes a diffuser with almost 0% specular transmittance. Thomas *et al.*[62] developed a similar tunable diffuser device based on graphene oxide (GO) films coated on silicone rubber membranes. This tunable diffuser works on the principle of delamination buckling of the GO film. Delamination occurs during a biaxial compression due to poor adhesion of the GO films to the silicone

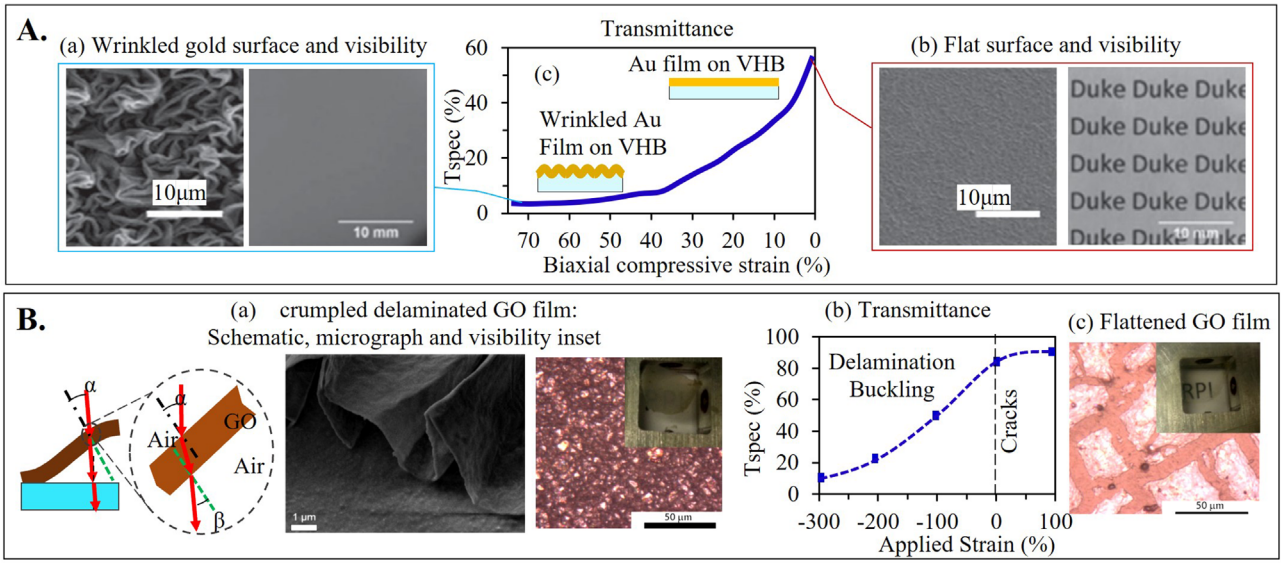

FIG. 11. (A) Formation of ridges by biaxial compression of VHB elastomer coated with a gold thin film. SEM micrograph and transmittance of the membranes at a biaxial compressive strain of (a) 67% and (b) 0%; (c) corresponding change in specular transmittance [Reproduced with permission from Cao *et al.*, Adv. Mater. **26**, 1763 (2014). Copyright 2014 John Wiley and Sons, Inc.].[63] (B) Buckling induced delamination of graphene oxide thin films as it is stretched to a fully flat state from a 300% biaxially compressed state: (a) illustrations, SEM micrograph of cross section, optical micrograph of surface and visibility through delamination buckled GO films; (b) cracks appears in the GO film at 400% strain as the tensile strain exceeds the pre-stretch applied before coating GO, yet the device appears more transparent; (c) specular transmittance while the delamination buckles are released [Reproduced with permission from Thomas *et al.*, Adv. Mater. **27**, 3256 (2015). Copyright 2015 John Wiley and Sons, Inc.].[62]

rubber substrate, which are buckled while the silicon rubber substrate itself remained flat [Fig. 11(B-a)]. When flat, this device shows greater than 90% transmittance. At the 400% uniaxially compressed stage, the device formed 4–5 μm amplitudes and 1–2 μm pitch delaminated ridges. The delaminated ridges of GO films slightly absorb and mostly scatter the incident beam [Fig. 11(B-b)]. Herein, the higher aspect ratio buckled patterns appeared hazier. With a 400% biaxial compression strain, this device lowers the transmittance to 10%.

Surface roughening can also be obtained by stretching an elastomer made of heterogeneous materials.[170] For instance, as shown in Figs. 12(a) and 12(b), through controlled stretching of porous soft materials filled with liquid of a similar refractive index, a virtual dynamic surface roughening effect can be obtained. Yao *et al.*[170] developed such a material that responded to a deformation of the elastomer substrate that changed the size of pores in the elastomer matrix. The fluid, that is, acting as a surface coating layer is drawn into the expanding pores or drawn out of the contracting pores. This suction or release of the surface fluid altered the surface topography accordingly. Yao *et al.*[170] used Teflon membranes made of the nanofiber as the porous matrix, which was supported by PDMS for mechanical integrity during stretching. A low surface energy fluid (DuPont Krytox 103 perfluoropolyether) capable of infiltrating the stretchable porous matrix was used as the surface covering liquid. As shown in Fig. 12(a) the surface covered by liquid appears transparent, stretch-induced driving in of the surface liquid exposed the pored and made the surface optically scattering.

b. Electrically controlled surface roughness using microwrinkles. Mechanically controlled uniaxial and biaxial wrinkling help visualize the concept and potential of tunable optical diffusers. Meanwhile, electrically tunable optically diffusive devices are attractive for practical applications due to the possibility of automation. A dielectric elastomer actuator (DEA) is one such a device capable of electrically unfolding pre-micro wrinkled electrodes. While the micro-wrinkled electrodes appear hazy, at the flat state, the compliant electrode for such DEA is optically clear [Fig. 13(A)]. Zang *et al.*[64] developed such a DEA device consisting of a pre-stretched dielectric elastomer membrane (3M VHB 4905) sandwiched between a pair of graphene coatings. As shown in Fig. 13(C), the device with a flat coating of 3–10 graphene layers on a 3–5 times biaxially pre-stretched substrate is highly transparent (80% transmittance). Upon partially releasing the pre-stretch, delamination and buckling of the graphene films occur yielding randomized wrinkles with a pitch of 0.2–2 μm. These wrinkles are smaller or comparable to the wavelength of visible light; hence, this device can merely mildly scatter light. Even a large uniaxial compression of 500% merely lowers the transmittance to 30%. However, employing the DEA, this device can electrically expand by 100% areal strain and unfold the ridges to increase transmittance to 60%.

To form large micro wrinkles via compression, the electrode material in the form of thin film needs to be stiffer (with high modulus) compared to the soft dielectric elastomer substrate [Eqs. (6) and (7)].[66] An indium tin oxide (ITO) film is a common choice of transparent electrodes for a touchscreen, and Ong *et al.*[65] showed the ITO film deposited by e-beam evaporation deposition on the acrylic elastomer membrane can make a crumpled complaint electrode. The films appeared slightly brownish and consisted of thermally induced micro-wrinkles. These thermally induced wrinkles of as-deposited ITO thin films turned the device mildly hazy (with 52% specular transmittance) even without the release of pre-stretch. Meanwhile, as the device is radially compressed by 14.2%, ITO films on the dielectric elastomer membrane are crumpled even more to become hazier. Hence, the specular transmittance is further reduced to 39%. By activating this ITO-based DEA device with a voltage of 6 kV, an areal actuation strain of 37% is obtained, which restores the device's specular transmittance to 52% [Fig. 13(D)].

Room-temperature e-beam evaporation promises conformal deposition of wrinkle-free optical films, such as optical metallic oxide on the elastomeric substrate. For example, optical metal oxides, such as ZnO and TiO_2, are preferred for high transmittance, high modulus, and high toughness.[66,172] Their nanometric coating on the soft elastomer results in a high modulus mismatch; hence, they can be readily buckled into large micro-wrinkles under a small compressive strain. These nanometric optical metal oxides are, however, insulators and they cannot make compliant electrodes by themselves for DEA.[66] As a simple solution, a conductive overcoat can be applied on the nanometric metal oxides to make micro-wrinkled compliant electrodes of variable specular transmittance. Figure 13(E) shows such a pair of multilayer electrodes of 10 nm thin silver (Ag) and 30 nm thick ZnO sandwiching a pre-stretched dielectric elastomer membrane; this makes a soft capacitor with 45% specular transmittance for 550 nm light.[67,169] Therein, the nanometric silver layer reduces the transmittance of the device even in the flat state. A 10% radial compression of the multi-layered nanometric thin films led to the formation of

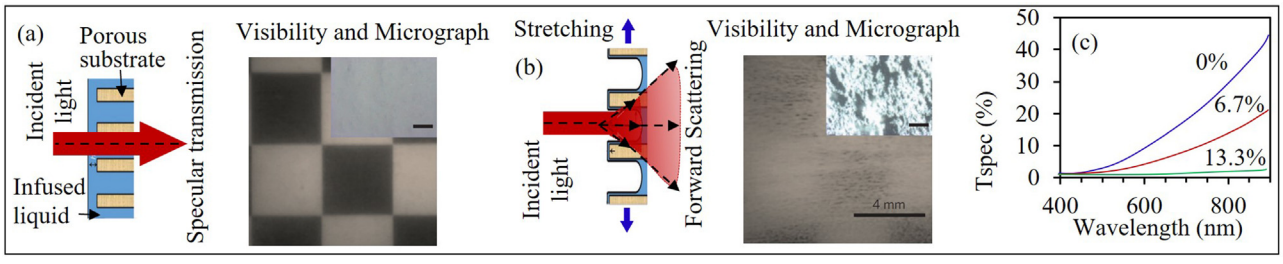

FIG. 12. Surface roughness variation through mechanical stretching of liquid-infused porous elastomer. Schematic showing exposure of micro-pores and light scattering upon stretching the fluid-infused elastomer membranes; (mid) visibility and micrograph of the nano-porous substrate made of nanofibrous Teflon network at the un-stretched and stretched state; (left) change in transmittance at various strain states [Reproduced with permission from Yao *et al.*, Nat. Mater. **12**, 529 (2013). Copyright 2013 Springer Nature].[170]

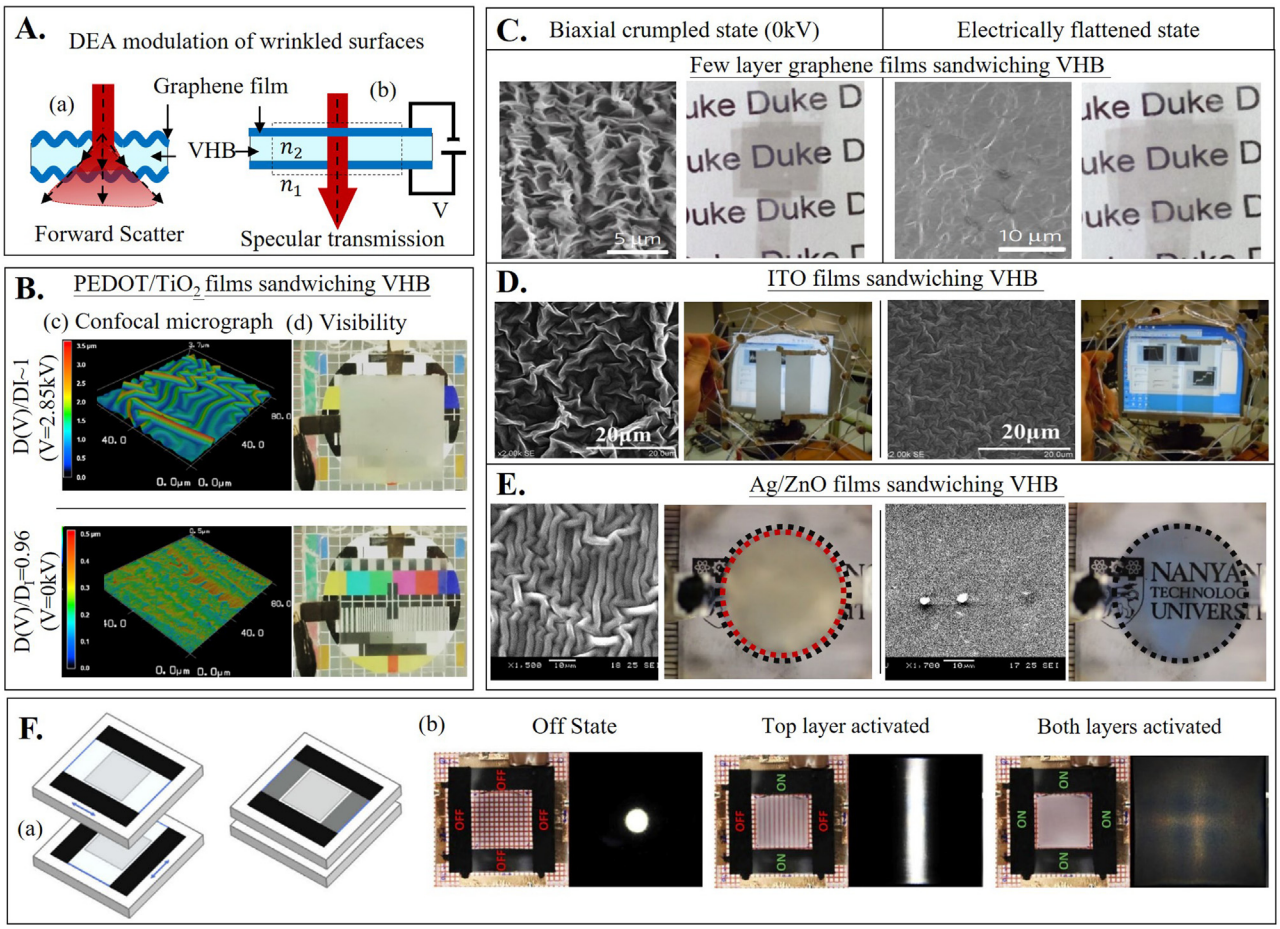

FIG. 13. Tuning transmittance by controlled biaxial micro wrinkling using DEA. (A) Schematic showing wrinkle control and light transmission using DEA. (B) Wrinkling and unfolding of the TiO_2/PEDOT:PSS electrode using DEA: confocal micrograph and visibility through the device at (a) wrinkled state [$D(V)/D_I = 0.96$] and (b) unwrinkled state with $D(V)/D_I = 1$ at 2.85 kV [Reproduced with the permission from Shrestha *et al.*, ACS Photonics **5**, 3255 (2018). Copyright 2018 American Chemical Society].[66] (C) DEA controlled wrinkling and unfolding of the graphene film-coated elastomer substrate: (left) SEM micrographs showing delamination wrinkling of graphene films and printed texts behind the device at the crumpled state; (right) SEM micrograph of the flattened graphene film and image seen through the device at the DEA-induced flattened state [Reproduced with permission from Zang *et al.*, Nat. Mater. **12**, 321 (2013). Copyright 2013 Springer Nature].[64] (D) SEM image of ITO and visibility through the ITO coated device at 14.2% crumpled state and 3% stretched state, which is also controlled using DEA [Reproduced with permission from Ong *et al.*, Appl. Phys. Lett. **107**, 132902 (2015). Copyright 2015 AIP Publishing].[65] (E) Wrinkling and unfolding of the Ag/ZnO thin film coated DEA: SEM micrograph and optical clarity at 10% radially compressed state and the flat state as DEA is activated [Reproduced with permission from Shrestha *et al.*, Proc. SPIE **10163**, 329 (2017). Copyright 2017 SPIE].[169] (F) Two overlapped devices with uniaxially wrinkable PEDOT/VHB/PEDOT layers with DEA forming orthogonal wrinkles for bi-directional light scattering: schematic of the device configuration, visibility through the device and scattering of light passing through the device as combinations of each layer are activated [Reproduced with permission from Chen *et al.*, Opt. Express **28**, 14 (2020). Copyright 2020 Optical Society of America].[171]

micro-wrinkles with a 3.35 μm pitch and 0.721 μm amplitude—making the micro wrinkled device highly translucent with only 1% specular transmittance throughout the visible spectrum. An activation with 6 kV unfolds the surface and restores the initial clarity. In comparison, a DEA device with 10 nm thick Ag-only as the electrodes merely formed sub-micrometer wrinkles. Even with 10% radial compression, the device merely produces a mild haze and is unable to conceal the image behind it. This comparison emphasizes the need for stiff thin films like ZnO to make a better optical diffuser.

Shrestha *et al.*[67] reported the inherent transmittance of the conductive thin film layer can impact the overall transmittance of the device. Therefore, a highly transparent conductive thin film layer in a multilayer electrode system can significantly improve the clear state of a device. For example, Fig. 13(B) shows a pair of multilayer electrodes made of PEDOT:PSS conductive film and TiO_2 film sandwiching a pre-stretched dielectric elastomer membrane, which makes an initially transparent DEA with 81% specular transmittance.[66] Moreover, 4% biaxial compression of the multi-layered nanometric oxide thin films leads to the formation of micro wrinkles with a 7–8 μm pitch and 0.585 μm amplitude. This microwrinkled device becomes highly translucent with only a 1.8% specular transmittance for broadband optical diffusion. An activation with 2.85 kV can unfold the surface and

restore the initial clarity. Chen *et al.*,[171,173] moreover, demonstrated two uniaxially wrinkling DEAs that are overlapping but the wrinkling direction is orthogonal to each other. As shown in Fig. 13(F), a pre-stretched VHB 4905 coated with PEDOT:PSS was utilized as the wrinkling component, and the carbon grease on the two sides of the DEA acts as the compressing component. Such a unique device demonstrates a directional scattering of light and possesses the potential to be used in many applications, for example, solar cells,[174] metamaterials, and nanoantenna devices.[175,176]

Table III summarizes the performance of various tunable optical diffusers based on microwrinkling. Current surface microwrinkling-based devices can switch from highly transparent (i.e., up to 90% transmission[61,62]) to highly translucent (i.e., up to 0%–1% transmission[63,67]) states and vice versa, which is mostly dependent on wrinkle dimensions. Furthermore, a low compression strain requirement (i.e., 0%–5%[66]) for microwrinkle formation promises large areal coverage and higher feasibility for real application as an actively tunable window. Hence, insight can be drawn by comparing these parameters for microwrinkling-based actively tunable window devices.

c. Inplane strain-free electrically induced surface micro-roughness. A mechanical compression can buckle a hard-coated elastomer to form surface wrinkles—but such operation is like folding a curtain, therefore, are less practical for a tunable window with a fixed size. Dielectric elastomer actuator, on the other hand, offers a means of the voltage-induced unfolding of the micro wrinkles; however, it still requires a large voltage-induced areal expansion.[64,66,171,173] This limits the active area for transmittance tuning to only a small areal fraction of the whole window. Preferably, surface wrinkling must occur to a bonded elastomer on the rigid support like glass panel without the need for axial compression. There have been a few research efforts to develop devices that are capable of surface roughening without in-plane strain. There are two approaches to these devices; First, voltage-induced surface instability of rigidly bonded rubber coated with thin-film electrodes;[177] Second, voltage-induced nanowire indentation of elastomer substrate coated with a percolative network of nanowires.[68,178–181]

van den Ende *et al.*[177] developed a new kind of switchable window that exploits voltage-induced surface instability to induce micro wrinkle to a rigidly bonded elastomer on a glass. This switchable window device consists of a transparent dielectric elastomer layer (acrylate

TABLE III. Comparison of the transmittance tunable windows using micro-wrinkling of a free elastomer.

S. no.	Coated thin film/coating method/(thickness)	Substrate (thickness)	Strain type and state (%)	Device area	Surface wrinkle amplitude and (pitch)	T_{spec} at 550 nm	References
1.	Gold/palladium (95%/5%)/sputtered/(11 nm)	PDMS (1 mm)	0%–27.5% (mechanical uniaxial strain)	$10 \times 40\ mm^2$	0.19 μm (1.21 μm)	···	160, 161
2.	Polyimide/bonded after treatment/ (7.5–12.5 μm)	PDMS (5 mm)	0%–5% (mechanical uniaxial strain)	$12 \times 12\ mm^2$	∼88 μm (∼680 μm)	90%	162
3.	Elastosil RT 625, wacker/spin coated/ (20 μm)	3M VHB 4910 (62.5 μm)	0%–32% (DEA induced uniaxial strain)	$3 \times 3\ mm^2$	(1–1.3 μm)	···	163
4.	Silicate/UVO and silane treated/	PDMS with nanopillars (1 mm)	0%–30% (mechanical uniaxial strain)	$40 \times 15\ mm^2$	4.4 μm (31 μm)	40%–90%	61
5.	Graphene oxide/drop casting/(20 nm)	Silicon rubber (0.5 mm)	100%–300% (mechanical areal strain)	$20 \times 20\ mm^2$	4–5 μm (1–2 μm)	10%–90%	62
6.	Gold/sputtered/ (13 nm)	3M VHB 4910 (250–62.5 μm)	0%–70% (mechanical biaxial strain)	$50 \times 50\ mm^2$	2–4 μm (8 μm)	0%–55%	63
7.	Graphene/transfer methods/(3–10 layer)	3M VHB 4905 (45–20 μm)	0%–100% (DEA areal actuation)	···	N/A (0.2–2 μm)	40%–60%	64
8.	Indium tin oxide (ITO)/evaporation deposition/(50 nm)	3M VHB 4905 (61.25 μm)	0%–37% (DEA areal actuation)	20 mm diameter	N/A (2–3 μm)	39.14%–52.08%	65
9.	TiO_2 and PEDOT:PSS/ evaporation deposition/spin coating/ (19.8/38.9 nm)	3M VHB 4905 (65 μm)	0%–5% (DEA radial actuation)	20 mm diameter	0.585 μm (7–8 μm)	81%–1.85%	66
10.	ZnO and Ag/evaporation deposition/ (30/10 nm)	3M VHB 4905 (65 μm)	0%–10% (DEA radial actuation)	20 mm diameter	1.443 μm (3.35 μm)	47%–1%	67
11.	PEDOT:PSS (<100 nm)	3M VHB 4905 (65 μm)	0%–10% (DEA biaxial actuation)	$60 \times 60\ mm^2$	0.4 μm (7–8 μm)	75%–4%	171

elastomer of low Young's modulus of 1.15 MPa, high dielectric constant of 20, and less than 25 μm thick), which is sandwiched by a flexible nanometric film of gold (42 nm thick) and an indium-tin-oxide (ITO) coated glass substrate (Fig. 14). At a voltage approaching critical voltage (345 V), which is applied across the two electrodes (one flexible and one rigid), electro-mechanical instability occurs at the surface with flexible electrodes, thus microwrinkles are formed making the device hazy [Fig. 14(b)]. The electromechanical instability occurs when the applied electric field surpasses the critical electrical field $E_c = \sqrt{\frac{\xi_c Y}{\varepsilon_o \varepsilon_r}}$, where ε_o, ε_r, and ξ_c are the vacuum permittivity, dielectric constant, and a experimentally evaluated function of the Poisson ratio of the elastomer.[182] Initially, in a flat state, the device's specular transmittance is only 37% due to the gold thin film. An activation voltage of 500 V is capable of roughening the surface up to RMS roughness of 600 nm, consequently reducing the specular transmittance to 33%. This limitation of these devices is the transmittance change obtainable is small as only a mild wrinkle could be formed due to the constraint by the rigid substrate in the lateral direction.

Instead of the metallic film, a percolative network of conductive nanotubes and/or nanowires can make a clearer and more compliant electrode.[178,179] It can be expected for a dense coating of carbon nanotube network (e.g., 100 nm thick) to appear dark; whereas, a sparse coating will appear relatively more transparent. A biaxial expansion can provide a means to tune the surface density of the network of carbon nanotube coated on the elastomer substrate and thus modulates the optical absorption [Fig. 15(A)]. Hu *et al.*[178] showed such voltage-induced area expansion can reduce the surface density to lighten the dark appearance of the coatings.[178] Surprisingly, DEA made of nanotube electrodes when activated blurred the logo (photo behind) despite causing a sparser network of carbon nanotubes.[178,179] A 5 kV activation of the device produces a 200% areal strain yet blurs out the logo and becomes hazy [Fig. 15(A-b)]. Later Shian and Clarke[180,181] used silver nanowires to show that the haziness of activated DEA is caused by nanoindentation of the elastomer substrate. The voltage-induced nano-indention roughens the elastomeric surface through the formation of micro-bulges producing a hazy appearance.

To understand the physics behind the formation of nano-indentation [Fig. 15(C-b)], consider a dielectric elastomer layer (thickness H, permittivity ε) bonded to the ITO layer of an ITO-coated glass and coated a network of nanowire of radius R. A voltage bias applied between the percolating network of nanowire and the bottom ITO electrode layer induces a 2D electrostatic field across the bonded dielectric elastomer layer. The electrostatic force per unit length of the nanowire acting along its normal direction is given by $\frac{F_n}{l} = \frac{\pi\varepsilon}{4a^2}\frac{V^2}{\left[\cosh^{-1}\left(\frac{H}{R}\right)\right]^2}$,[181] where $a = 1/2\left(H + \sqrt{H^2 - R^2}\right)$. The electrostatic force, that is, concentrated beneath the nanowire locally indents the bonded dielectric elastomer layer. As opposite reaction such indentation causes elastomeric deformation to form micro-bulges on the free side of the elastomer. The indentation and micro-bulges roughen the elastomeric surface, thus diffusing the transmitting light. Figure 15(C) shows a dielectric layer capacitor that consists of a pre-stretched acrylic elastomer membrane (3M VHB 4905). The membrane is sandwiched between an ITO layer of the ITO-coated glass and a silver nanowire mat (of 78 mg/m^2 areal density). As an electric field of 96 V/μm is applied to activate this device, the silver nanowires indent the soft elastomer surface and cause sub-micron bulging of 600 nm peak-to-valley heights. This device is only 70% transparent in the inactive state because the network of silver nanowires (90 nm diameter and 20–60 μm length) significantly scatters incident light. Voltage activation modulates the device to be hazier with a mere 20% inline transmittance.[181]

The haziness of a tunable elastomeric optical diffuser can be increased by using double variable roughness layers, instead of using a single layer. For example, a soft capacitor made of triple-dielectric laminates sandwiched by pair of nanowire-based electrodes, where the laminate is made of the acrylate dielectric elastomer layers (3.1 μm thick and 450 kPa modulus) sandwiching a middle Mylar layer (13 μm thick and 5.2 GPa). The haziness is increased even in the inactive state [Fig. 15(B)].[180] The elastomeric films were prepared from four times

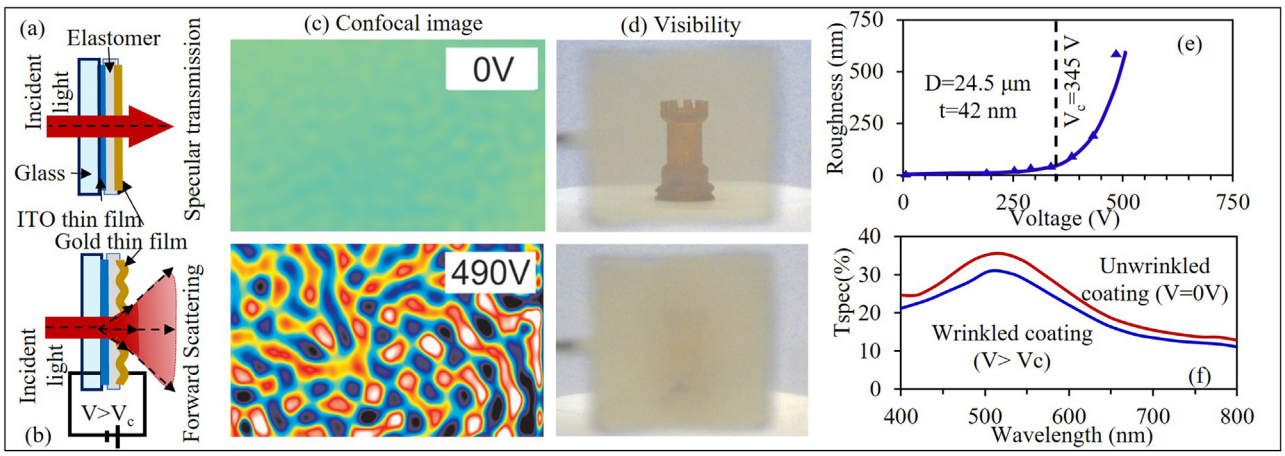

FIG. 14. Change in surface roughness by voltage-induced surface instability of a DEA bonded to the glass. Schematic of the device: (a) at off state; (b) at on state; (c) corresponding surface topography of the device and (d) visibility of the chess piece behind the device (light is scattered by roughened surface and the object is almost concealed); (e) evolution of the surface roughness as voltage exceeds the critical voltage; and (f) change in transmittance spectrum by voltage activation [Reproduced with permission from van den Ende *et al.*, Adv. Mater. **25**, 3438 (2013). Copyright 2013 John Wiley and Sons, Inc.].[177]

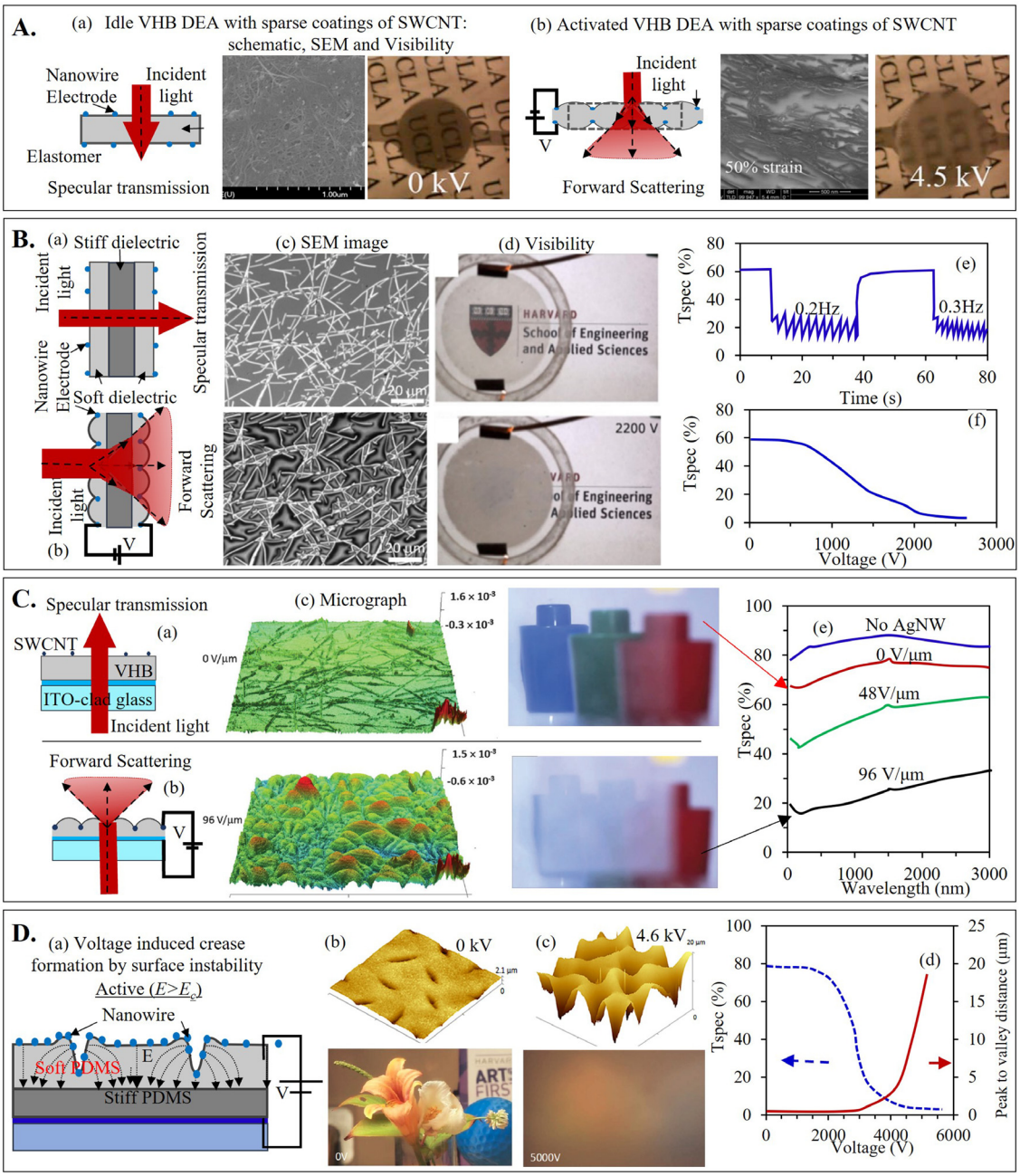

FIG. 15. Scattering light by roughening surface through voltage-induced indentation of elastomer by nanowire electrodes. (A) Indentation of the surface of a free elastomer membrane by activation of Single-Walled Carbon Nanotubes (SWCNT) network-based DEA. Schematic, SEM and visibility through the device: (a) at inactive state; (b) as the DEA is activated [Reproduced with permission from Hu *et al.*, Appl. Phys. Lett. **94**, 161108 (2009). Copyright 2009 AIP Publishing.[178] Reproduced with permission from Yuan *et al.*, Adv. Mater. **20**, 621 (2008). Copyright 2008 John Wiley and Sons, Inc.].[179] (B) Double variable roughness layers made of a stiff dielectric layer sandwiched between the soft dielectric layer with the AgNW network as a compliant electrode. Schematic at (a) off state, (b) on state, (c) SEM micrograph at off state and on state with 125 MV/m electric field, (d) visibility through the device at 0 and 2200 V, (e) change in specular transmission at 550 nm wavelength with AC voltage activation, and (f) gradual decrease in transmittance with increasing voltage [Reproduced with permission from Shian *et al.*, Opt. Lett. **41**, 1289 (2016). Copyright 2016 Optica Publishing Group].[180] (C) Single variable roughness layers with the dielectric layer bonded to ITO coated glass and SWCNT network as the indenting electrode. Schematic at (a) off state, (b) on state, (c) confocal micrograph and corresponding visibility at off state and on state, and (d) change in specular transmittance at various electric-field [Reproduced with permission from Shian *et al.*, Soft Matter **12**, 3137 (2016). Copyright 2016 Royal Society of Chemistry].[181] (D) Surface instability induced roughness with the CNT network as an electrode. (a) Schematic of the device with surface instability at the electric field above E_c; surface micrograph and visibility through the device at (b) inactive state, (c) 4.6 kV with surface instability induced roughness, and (d) modulation of inline transmittance obtained by the corresponding change in voltage-induced roughness [Reproduced with permission from Shian *et al.*, J. Appl. Phys. **123**, 113105 (2018). Copyright 2018 AIP Publishing].[68]

biaxially pre-stretched acrylic adhesive tapes (3M VHB F9460PC). The electrode cladding is a coating of percolating network of the silver nanowire with 78 mg/m^2 areal density. At off state, the laminate capacitive device is clear with 62% specular transmittance, while at on-state [2.4 kV (125 V/μm) dynamic activation at 3 Hz], the surface roughens to reduce the specular transmittance down to 8% [Figs. 15(C-e) and 15(C-f)]. The challenge with this device is the drift in the transmittance at the activated state if AC high voltage is not used for activation.

Ideally, a tunable optical diffuser can switch between clear and frosted. The tunable devices based on silver nanowires are initially not so clear.[180,181] As a solution, Shian *et al.*[68] used a space network of single-walled carbon nanotubes with a diameter of 4–5 nm to make a more transparent device at the inactive states [Fig. 15(D)]. The device is a soft capacitor consisting of two laminated dielectric elastomers; a top layer of a sparse network of nanowire-coated soft silicone (160 μm thick and 7 kPa shear modulus) and a middle layer of hard silicone (55 μm thick and 700 kPa shear modulus) on an ITO-coated glass are highly transparent (80% specular transmittance) [Fig. 15(D-b)]. High-voltage activation of the device reduced the transmittance characterized by (1) a gradual decrease in transmittance caused by nano-indentation and consequently formed surface bulges at a lower voltage and (2) a drastic decrease in transmittance caused by surface instability as the activation voltage surpasses critical voltage.[182] At the critical voltage (4600 V), the top/free surface is roughened with the formation of ridges of 250 μm pitch and a 19 μm peak-to-valley height; These large ridges reduce specular transmittance down to 8%. Through, the device enables a wide range modulation of transmittance from 80% to 8%, the deactivation is subjected to substantial hysteresis and recovery takes a long period. Compared to other nanowire or nanotube-based tunable window devices, these devices could reach a more hazy state because of surface instabilities that induce higher RMS roughness (Table IV).

In summary, transmittance tunable windows based on variable surface roughness are promising because of their simple construction, low energy consumption, and large transmittance modulation range. They can be broadly divided into two types depending on the need for compression strain to tune transmittance. Figure 16(a) compares microwrinkling devices (needs compression strain) in terms of optical modulation capability and area strain requirement. For real applications, a larger transmittance modulation range and small area strain requirement are desired. Thus far, a single electrode film is not capable of fulfilling the requirement of high transmittance, high stiffness, toughness, and electrical conductivity; it is, therefore, observed multilayered system such as TiO_2/PEDOT:PSS offers better performance for microwrinkle-based tunable windows. Ideally, transmittance tuning without compression strain is desired in real applications. Therefore, the device based on electrically induced surface microroughness possesses higher potential than that of microwrinkles-based devices. Figure 16(b) compares such devices that can be bonded to a rigid substrate in terms of transmittance modulation range and electric field requirements. It is seen that the devices using thin films have poor transmittance modulation range compared to ones using nanowires. Furthermore, the device using a nanowire sheet with higher transmittance and harnessing the electromechanical instability to obtain large surface roughness demonstrates optimum performance in terms of both transmittance modulation as well as electric field requirement.[68,183]

IV. CONCLUSIONS AND OUTLOOK

Optical transmittance tunable windows can be used to promote daylighting and visual privacy preservation as desired. Therefore, energy-saving and enhancing indoor comforts can be appreciated by incorporating tunable windows in the buildings. In this review, we comprehensively presented an overview of various types of actively tunable windows. Herein, we categorized such tunable windows based on the optics involved and further sub-categorized them based on the stimulus needed to obtain dynamic properties. There are a few commercially available window devices with tunable transmittance based on

TABLE IV. Comparison of the transmittance tunable windows based on nanowires on the bonded elastomer.

Single/multilayer substrate (shear modulus)	Substrate area (thickness)	Dielectric constant	Electrodes (dimension)/coating method/	Applied electric field, E	Surface property	$T_{spec\ at\ 550\ nm}$ inactive	$T_{spec\ at\ 550\ nm}$ active	Reference
Single layer acrylate elastomer (~380 kPa)	15 × 15 mm^2 (4–23 μm)	20	Gold (42–336 nm thick)/evaporation deposition/and ITO	14 V/μm	2 A–2 μm $p \sim$ 10–30 μm	37%	33%	177
Single-layer 3M VHB4905 (600 kPa)	−(31 μm)	4.7	AgNW (ϕ = 90 nm; 20–60 μm length)/ ITO/transfer method/	96 V/μm	2 A–0.6 μm $p \sim$ 3 μm	70%	20%	181
Triple layer 3M VHBF9460PC/Mylar/ VHBF9460PC (600 kPa)	−(3.1/13/ 3.1 μm)	2.92	AgNW (ϕ = 90 nm; 20–60 μm length)	125 V/μm	N/A	62%	8%	180
Double layer sylgard184 10:1/sylgard184 50:1 (700 kPa/7 kPa)	47 mm diameter (50/160 μm)	2.68	CNT (ϕ = 4–5 nm; 0.5–1.5 μm length)/ spraying/filtration-stamping method/ and ITO	33.3 V/μm	2 A–19 μm $p \sim$ 250 μm	80%	8%	68, 183

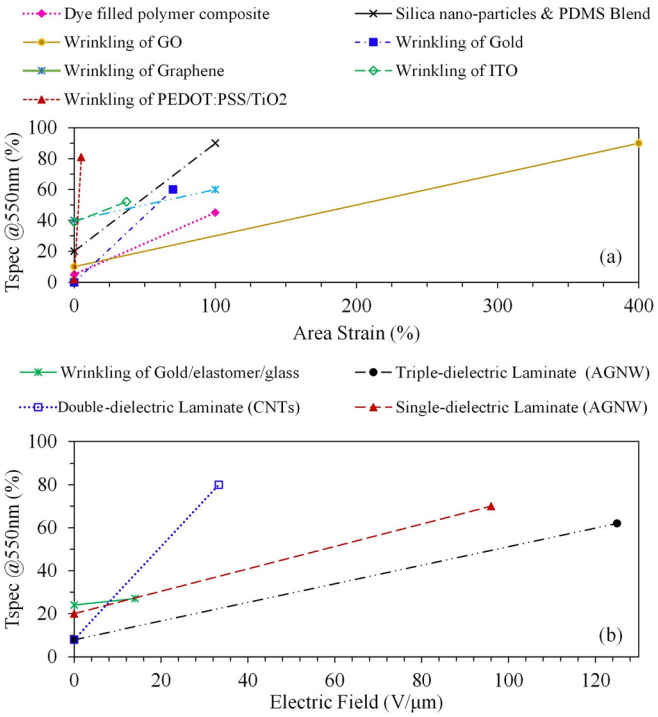

FIG. 16. Comparison of different technologies of transmittance tunable windows, which involves (a) area strain and (b) the elastomer layer bonded to a rigid substrate.

(or a combination of) electrochromic glasses or PDLC or SPD technology. However, most of them are expensive to fit into a wider commercial window market. Therefore, current state-of-the-art technologies as highlighted in this review show potential as an alternative tunable window for the future.

The new concepts of low-cost technologies for tunable windows work on various optical principles as we categorize them, namely, (a) light absorption, (b) light reflection, and (c) diffuse transmission. As comprehensively summarized, the emerging alternative tunable window devices also possess their pros and cons. The device based on the light-absorbing particles-filled polymer composites needs high mechanical strain just to obtain a moderate transmittance tuning range. Meanwhile, optofluidic devices involve fluid pumping in and out of a chamber—despite having a large transmittance tuning range, these devices involving liquids are prone to leakage. Tunable optical diffusers, on the other hand, are a promising class of low-cost active window devices. They are categorized into two groups based on the types of substrate used, namely, (a) free elastomeric membrane and (b) bonded rubber on a rigid substrate. The free membrane devices are based on variable air-void densities or based on surface roughening upon the large mechanical stretch. The tunable windows based on thin-film wrinkling show a wide range of transmittance tuning. Micro-wrinkle formation under a small strain is, however, required to enable larger active area coverage for the transmittance tuning. The device based on bonded rubber does not require a stretch for transmittance tuning and such a device can provide a decent range of transmittance tuning by voltage-induced nano-indentation or electromechanical instabilities. However, some improvements on the default appearance of such devices need to be performed as they are laminated with a percolative network of nanowire as electrodes and they can be slightly hazy.

There is a big room for performance enhancements of the emerging alternative tunable windows in terms of transmittance modulation range and power consumption. In addition, further studies are needed to make them less expensive, more robust, and simpler to manufacture as well as operate. The price factor can be improved by increasing the energy-saving efficiency of tunable windows as well as reducing energy consumption to operate them. Another main concern is the need for long-term durability. The development of stable materials and methods are needed to improve the performance and stabilities of materials and structures. In addition, tunable window research must focus on industrially scalable manufacturing aspects. The development of a successful transmittance tunable window needs to focus on interdisciplinary areas. It involves material engineering, optics, electrical and electronics and industrial manufacturing aspects. It is hoped that this review provokes attention from different areas including both academic and industrial research to accelerate the development of industrially manufacturable, commercially available and economically acceptable smart tunable windows.

ACKNOWLEDGMENTS

This research was supported by the Singapore Millennium Foundation managed by Temasek Foundation Innovates and by Temasek Foundation Ecosperity. This study was supported under the RIE2020 Industry Alignment Fund—Industry Collaboration Projects (IAF-ICP) Funding Initiative, as well as cash and in-kind contribution from the industry partner(s).

AUTHOR DECLARATIONS

Conflict of Interest

The authors have no conflicts to disclose.

Author Contributions

Milan Shrestha: Conceptualization (lead); Data curation (lead); Formal analysis (lead); Investigation (lead); Validation (lead); Visualization (lead); Writing – original draft (lead); Writing – review and editing (lead). **Gih-Keong Lau:** Conceptualization (equal); Data curation (equal); Formal analysis (equal); Validation (equal); Visualization (equal); Writing – original draft (equal); Writing – review and editing (equal). **Anil Kumar Bastola:** Data curation (supporting); Writing – original draft (supporting); Writing – review and editing (supporting). **Zhenbo Lu:** Conceptualization (supporting); Writing – original draft (supporting). **Anand Asundi:** Conceptualization (supporting); Data curation (supporting); Writing – original draft (supporting). **Edwin Hang Tong Teo:** Validation (supporting); Writing – review and editing (supporting).

DATA AVAILABILITY

The data that support the findings of this study are available from the corresponding author upon reasonable request. The data that support the findings in others' publications and are presented in this review are available from the corresponding authors of publications cited in this review. Restrictions may apply to the availability of these data.

NOMENCLATURE

Acronyms

A	absorbance
A	wrinkle amplitude
AFM	atomic force microscopy
DEA	dielectric elastomer actuators
e	compressive strain
e_c	critical buckling strain
E_c	critical electrical field
E_f	Young's modulus of the film
E_s	Young's modulus of the substrate
GO	graphene oxide
HVAC	heating, ventilation, and air conditioning
ITO	indium tin oxide
I_o	intensity of incident light
I_{spec}	intensity of specularly transmitted light
LCE	liquid crystal elastomer
MEMS	micro-electromechanical system
NIR	near-infrared
PDLC	polymer dispersed liquid crystal devices
PDMS	polydimethylsiloxane
PEDOT:PSS	poly(3,4-ethylenedioxythiophene) polystyrene sulfonate
PET	polyethylene terephthalate
PMANa	poly methacrylic acid sodium salt
PS	polystyrene
PU	polyurethane
PVA	polyvinyl alcohol
R	reflectance
SEM	scanning electron microscope
SPD	suspended particle devices
t	optical thickness of the absorbent medium
t_f	thickness of surface films
T	transmittance
TIS	total integrated scattering
T_{spec}	specular transmittance
UV	ultraviolet
ε_o	vacuum permittivity
ε_r	dielectric constant
η	refractive index
θ_c	critical angle
μ	linear attenuation coefficient
ν	Poisson's ratio
σ	rms surface roughness
3M VHB	double-sided foam tapes from company 3M™

REFERENCES

[1]A. Piccolo and F. Simone, J. Build. Eng. **3**, 94 (2015).
[2]F. Asdrubali, M. Bonaut, M. Battisti, and M. Venegas, Energy Build. **40**, 1805 (2008).
[3]E. Syrrakou, S. Papaefthimiou, and P. Yianoulis, Sci. Total Environ. **359**, 267 (2006).
[4]H. Shahnazari, P. Mhaskar, J. M. House, and T. I. Salsbury, Comput. Chem. Eng. **108**, 139 (2018).
[5]S. Grynning, A. Gustavsen, B. Time, and B. P. Jelle, Energy Build. **61**, 185 (2013).
[6]R. A. Mangkuto, M. Rohmah, and A. D. Asri, Appl. Energy **164**, 211 (2016).
[7]S. Zhang, W. Hu, D. Li, C. Zhang, M. Arıcı, Ç. Yıldız, X. Zhang, and Y. Ma, Energy **222**, 119916 (2021).
[8]Y. Ke, J. Chen, G. Lin, S. Wang, Y. Zhou, J. Yin, P. S. Lee, and Y. Long, Adv. Energy Mater. **9**, 1902066 (2019).
[9]Y. Zhou, X. Dong, Y. Mi, F. Fan, Q. Xu, H. Zhao, S. Wang, and Y. Long, J. Mater. Chem. A **8**, 10007 (2020).
[10]H. Li, W. Zhang, and A. Y. Elezzabi, Adv. Mater. **32**, 2003574 (2020).
[11]K. Khaled and U. Berardi, Energy Build. **244**, 111022 (2021).
[12]C. Zhou, D. Li, Y. Tan, Y. Ke, S. Wang, Y. Zhou, G. Liu, S. Wu, J. Peng, and A. Li, Adv. Opt. Mater. **8**, 2000013 (2020).
[13]R. Tällberg, B. P. Jelle, R. Loonen, T. Gao, and M. Hamdy, Sol. Energy Mater. Sol. Cells **200**, 109828 (2019).
[14]P. Bamfield, *Chromic Phenomena: Technological Applications of Colour Chemistry* (Royal Society of Chemistry, 2010).
[15]O. Srirodpai, J. Wootthikanokkhan, S. Nawalertpanya, K. Yuwawech, and V. Meeyoo, Materials **10**, 53 (2017).
[16]T. T. Dao, S. Park, S. Sarwar, H. Van Tran, S. I. Lee, H. S. Park, S. H. Song, H. D. Nguyen, K.-K. Lee, and C.-H. Han, Sol. Energy Mater. Sol. Cells **231**, 111316 (2021).
[17]M. Aburas, V. Soebarto, T. Williamson, R. Liang, H. Ebendorff-Heidepriem, and Y. Wu, Appl. Energy **255**, 113522 (2019).
[18]A. Cannavale, G. Zampini, F. Carlucci, M. Pugliese, F. Martellotta, U. Ayr, V. Maiorano, F. Ortica, F. Fiorito, and L. Latterini, Sol. Energy (published online).
[19]C. Sol, J. Schläfer, I. P. Parkin, and I. Papakonstantinou, Sci. Rep. **8**(1), 13249 (2018).
[20]T. D. Vu, Z. Chen, X. Zeng, M. Jiang, S. Liu, Y. Gao, and Y. Long, J. Mater. Chem. C **7**, 2121 (2019).
[21]Y. Zhang, C. Y. Tso, J. S. Iñigo, S. Liu, H. Miyazaki, C. Y. H. Chao, and K. M. Yu, Appl. Energy **254**, 113690 (2019).
[22]S. Wang, Y. Zhou, T. Jiang, R. Yang, G. Tan, and Y. Long, Nano Energy **89**, 106440 (2021).
[23]B. P. Jelle, Sol. Energy Mater. Sol. Cells **116**, 291 (2013).
[24]G. Yang, Y.-M. Zhang, Y. Cai, B. Yang, C. Gu, and S. X.-A. Zhang, Chem. Soc. Rev. **49**, 8687 (2020).
[25]H. Ling, J. Wu, F. Su, Y. Tian, and Y. J. Liu, Nat. Commun. **12**(1), 1010 (2021).
[26]S. Fathi and A. Kavoosi, Sol. Energy **223**, 132 (2021).
[27]X. Jia, E. C. Baird, J. Blochwitz-Nimoth, S. Reineke, K. Vandewal, and D. Spoltore, Nano Energy **89**, 106404 (2021).
[28]A. Ghosh and B. Norton, Renewable Energy **126**, 1003 (2018).
[29]S. Mikhailova, L. Mikhailov, G. Ismailova, N. Kenes, R. Yersaiyn, and R. Mahmutov, Mater. Today: Proc. **49**, 2527 (2022).
[30]D. Cupelli, F. P. Nicoletta, S. Manfredi, M. Vivacqua, P. Formoso, G. D. Filpo, and G. Chidichimo, Sol. Energy Mater. Sol. Cells **93**, 2008 (2009).
[31]M. Kim, K. J. Park, S. Seok, J. M. Ok, H.-T. Jung, J. Choe, and D. H. Kim, ACS Appl. Mater. Interfaces **7**, 17904 (2015).
[32]L. Jinqian, Y. Zhao, H. Gao, D. Wang, Z. Miao, H. Cao, Z. Yang, and W. He, Liq. Cryst. **49**(1), 29–38 (2021).
[33]M. Khalid, K. Shanks, A. Ghosh, A. Tahir, S. Sundaram, and T. K. Mallick, Renewable Energy **164**, 96 (2021).
[34]G. Gorgolis and D. Karamanis, Sol. Energy Mater. Sol. Cells **144**, 559 (2016).
[35]M. Kamalisarvestani, R. Saidur, S. Mekhilef, and F. S. Javadi, Renewable Sustainable Energy Rev. **26**, 353 (2013).
[36]M. Cannistraro, M. E. Castelluccio, and D. Germanò, J. Build. Eng. **19**, 295 (2018).
[37]R. J. De Dear and G. S. Brager, Energy Build. **34**, 549 (2002).
[38]M. Han, R. May, X. Zhang, X. Wang, S. Pan, Y. Da, and Y. Jin, Sustainable Cities Soc. **61**, 102247 (2020).
[39]P. P. Murmu, A. Shettigar, S. V. Chong, Z. Liu, D. Goodacre, V. Jovic, T. Mori, K. E. Smith, and J. Kennedy, J. Materiomics **7**, 612 (2021).
[40]P. P. Murmu, V. Karthik, Z. Liu, V. Jovic, T. Mori, W. L. Yang, K. E. Smith, and J. V. Kennedy, ACS Appl. Energy Mater. **3**, 10037 (2020).
[41]J. Yin, J. Li, L. Wang, B. Cai, X. Yang, X. Li, and W. Lü, J. Energy Storage **51**, 104460 (2022).
[42]G. Syrrokostas, G. Leftheriotis, and S. N. Yannopoulos, Renewable Sustainable Energy Rev. **162**, 112462 (2022).
[43]L. Lavagna, G. Syrrokostas, L. Fagiolari, J. Amici, C. Francia, S. Bodoardo, G. Leftheriotis, and F. Bella, J. Mater. Chem. A **9**, 19687 (2021).

[44]A. Dokouzis, F. Bella, K. Theodosiou, C. Gerbaldi, and G. Leftheriotis, Mater. Today Energy **15**, 100365 (2020).
[45]C.-Y. Cheng, Y.-J. Chiang, H.-F. Yu, L.-Y. Hsiao, C.-L. Yeh, L.-Y. Chang, K.-C. Ho, and M.-H. Yeh, Nano Energy **90**, 106575 (2021).
[46]K. C. Lanigan, W. Jeong, M. A. Gerges, and M. Ahmed, J. Photochem. Photobiol., A **433**, 114117 (2022).
[47]Y. Zhou, F. Fan, Y. Liu, S. Zhao, Q. Xu, S. Wang, D. Luo, and Y. Long, Nano Energy **90**, 106613 (2021).
[48]D. Cho, H. Chen, J. Shin, and S. Jeon, Nanophotonics **11**, 2737 (2021).
[49]Y. Wang, E. L. Runnerstrom, and D. J. Milliron, Annu. Rev. Chem. Biomol Eng. **7**, 283 (2016).
[50]R. Baetens, B. P. Jelle, and A. Gustavsen, Sol. Energy Mater. Sol. Cells **94**, 87 (2010).
[51]S. Wang, W. Gao, X.-Y. Hu, Y.-Z. Shen, and L. Wang, Chem. Commun. **55**, 4137 (2019).
[52]J. Scarminio, A. Urbano, and B. Gardes, Mater. Chem. Phys. **61**, 143 (1999).
[53]S. Kandpal, T. Ghosh, M. Sharma, D. K. Pathak, M. Tanwar, C. Rani, R. Bhatia, I. Sameera, A. Chaudhary, and R. Kumar, Appl. Phys. Lett. **118**, 153301 (2021).
[54]H. Gong, W. Li, G. Fu, Q. Zhang, J. Liu, Y. Jin, and H. Wang, J. Mater. Chem. A **10**, 6269–6290 (2022).
[55]Y. Zhai, J. Li, S. Shen, Z. Zhu, S. Mao, X. Xiao, C. Zhu, J. Tang, X. Lu, and J. Chen, Adv. Funct. Mater. **32**, 2109848 (2022).
[56]R. Kumar, D. K. Pathak, and A. Chaudhary, J. Phys. D: Appl. Phys. **54**, 503002 (2021).
[57]D. Wolfe and K. W. Goossen, Opt. Express **26**, A85 (2017).
[58]F. Ahmad, M. Luqman, and M. Jamil, Mol. Cryst. Liq. Cryst. **731**, 1 (2021).
[59]S. Khosla, S. Lal, and A. Devi, in *Review of Blue Phase Liquid Crystal Devices* (AIP Publishing LLC, 2021), p. 020037.
[60]B. Li, Y. Wu, Y. Sun, W. Ma, L. Jiang, Z. Yang, F. Li, and G. Chen, Appl. Phys. Lett. **119**, 264103 (2021).
[61]S. G. Lee, D. Y. Lee, H. S. Lim, D. H. Lee, S. Lee, and K. Cho, Adv. Mater. **22**, 5013 (2010).
[62]A. V. Thomas, B. C. Andow, S. Suresh, O. Eksik, J. Yin, A. H. Dyson, and N. Koratkar, Adv. Mater. **27**, 3256 (2015).
[63]C. Cao, H. F. Chan, J. Zang, K. W. Leong, and X. Zhao, Adv. Mater. **26**, 1763 (2014).
[64]J. Zang, S. Ryu, N. Pugno, Q. Wang, Q. Tu, M. J. Buehler, and X. Zhao, Nat. Mater. **12**, 321 (2013).
[65]H.-Y. Ong, M. Shrestha, and G.-K. Lau, Appl. Phys. Lett. **107**, 132902 (2015).
[66]M. Shrestha, A. Asundi, and G.-K. Lau, ACS Photonics **5**, 3255 (2018).
[67]M. Shrestha, A. Asundi, and G.-K. Lau, in *Electrically Tunable Window Based on Microwrinkled ZnO/Ag Thin Film* (International Society for Optics and Photonics, 2017), p. 101631Y.
[68]S. Shian, P. Kjeer, and D. R. Clarke, J. Appl. Phys. **123**, 113105 (2018).
[69]J. M. Palmer, *Handbook of Optics* (McGraw-Hill, 1995), Vol. **2**, p. 251.
[70]E. C. Fest and S. O. P.-O. I. Engineers, *Stray Light Analysis and Control* (SPIE Press, Bellingham, 2013).
[71]J. Flammer, M. Mozaffarieh, and H. Bebie, *Basic Sciences in Ophthalmology* (Springer, 2013), Ed. 1, p. 21.
[72]S. Shaik, K. Gorantla, S. Mishra, and K. S. Kulkarni, Constr. Build. Mater. **263**, 120155 (2020).
[73]W. Wu, M. Wang, J. Ma, Y. Cao, and Y. Deng, Adv. Electron. Mater. **4**, 1800185 (2018).
[74]A. Cannavale, U. Ayr, F. Fiorito, and F. Martellotta, Energies **13**, 1449 (2020).
[75]U. Wang, *Making Smart Windows that Are Also Cheap*; available at https://www.technologyreview.com/2010/08/13/201564/making-smart-windows-that-are-also-cheap (MIT Technology Review, 2010).
[76]R. Skorpil, *How Much Do Smart Windows Cost?*; available at https://modernize.com/homeowner-resources/windows/smart-windows-cost (Modernize, 2022).
[77]H. N. Kim and S. Yang, Adv. Funct. Mater. **30**, 1902597 (2020).
[78]K. V. Wong and R. Chan, J. Energy Resour. Technol. **136**, 012002 (2014).
[79]A. Pawlicka, Recent Pat. Nanotechnol. **3**, 177 (2009).
[80]Saint-Gobain, *Smart Glass for Better Buildings;* available at https://www.sageglass.com/en/products.
[81]Lawrence Berkeley National Laboratory, *Soladigm Electrochromic Glass Layers*; available at https://windows.lbl.gov/tools/knowledge-base/articles/soladigm.
[82]*Say Goodbye to Blinds;* available at https://view.com/product.
[83]S. D. Rezaei, S. Shannigrahi, and S. Ramakrishna, Sol. Energy Mater. Sol. Cells **159**, 26 (2017).
[84]C. M. Lampert, Thin Solid Films **236**, 6 (1993).
[85]A. Chaudhary, D. K. Pathak, M. Tanwar, P. Yogi, P. R. Sagdeo, and R. Kumar, ACS Appl. Electron. Mater. **1**, 58 (2019).
[86]C. G. Granqvist, Thin Solid Films **564**, 1 (2014).
[87]Smart Tint, *Smart Tint;* available at https://www.smarttint.com/.
[88]Gauzy, "LCG® Smart Glass;" available at https://www.gauzy.com/products/.
[89]P. Display, "Switchable smart glass;" available at https://prodisplay.com/smart-glass/switchable-smart-glass/switchable-smart-glass/.
[90]Homestratosphere, "20 top smart home window solutions;" available at https://www.homestratosphere.com/smart-home-window-solutions/.
[91]J. W. Doane, N. A. Vaz, B. G. Wu, and S. Žumer, Appl. Phys. Lett. **48**, 269 (1986).
[92]J. W. Doane, MRS Bull. **16**, 22 (2013).
[93]L. Jun, W. Chien-Hui, S. Gauza, R. Lu, and W. Shin-Tson, J. Disp. Technol. **1**, 51 (2005).
[94]S. Denko, "SPD Film - 'LCF-1103DHA';" available at https://www.ma.showadenko.com/products_ppcm_11.htm.
[95]R. Frontiers, "SPD-Smartglass;" available at https://www.smartglass.com/#overview-section.
[96]R. Vergaz, J. Pena, D. Barrios, I. Pérez, and J. Torres, Opto-Electron. Rev. **15**, 154 (2007).
[97]S. Chakrapani and S. M. Slovak, Google patents (2001).
[98]A. Ghosh, B. Norton, and A. Duffy, Appl. Energy **159**, 362 (2015).
[99]S. Nundy and A. Ghosh, Renewable Energy **156**, 1361 (2020).
[100]A. Beer, Ann. Phys. **162**, 78 (1852).
[101]M. Fox, "Optical properties of solids" (American Association of Physics Teachers, 2002).
[102]F. López Jiménez, S. Kumar, and P. M. Reis, Adv. Opt. Mater. **4**, 620 (2016).
[103]J. Yang, H. Lee, S. G. Heo, S. Kang, H. Lee, C. H. Lee, and H. Yoon, Adv. Mater. Technol. **4**, 1900140 (2019).
[104]B. P. Heiz, Z. Pan, L. Su, S. T. Le, and L. Wondraczek, Adv. Sustainable Syst. **2**, 1700140 (2018).
[105]F. L. Jiménez, P. Upadhyaya, J. Liljenhjerte, P. M. Reis, and S. Kumar, Extreme Mech. Lett. **9**, 297 (2016).
[106]B. P. Heiz, Z. Pan, G. Lautenschläger, C. Sirtl, M. Kraus, and L. Wondraczek, Adv. Sci. **4**, 1600362 (2017).
[107]Z. Yang, J. K. Park, and S. Kim, Small **14**, 1702839 (2018).
[108]Y. J. Seo, H. G. Lee, J. S. Yang, H. Jeong, J. Han, J.-H. Kim, H.-J. Koo, and H. Yoon, RSC Adv. **11**, 2390 (2021).
[109]J. Li, X. Lu, Y. Zhang, F. Cheng, Y. Li, X. Wen, and S. Yang, ACS Appl. Mater. Interfaces **12**, 31637 (2020).
[110]F. P. Miller, A. F. Vandome, and M. B. John, *Fresnel Equations* (VDM Publishing, 2010).
[111]G. Woan, *The Cambridge Handbook of Physics Formulas* (Cambridge University Press, 2000).
[112]P. H. Notten, Curr. Opin. Solid State Mater. Sci. **4**, 5 (1999).
[113]A.-M. Janner, P. van der Sluis, and V. Mercier, Electrochim. Acta **46**, 2173 (2001).
[114]K. Ng, F. Zhang, V. Anisimov, and T. Rice, Phys. Rev. B **59**, 5398 (1999).
[115]A. Remhof and A. Borgschulte, ChemPhysChem **9**, 2440 (2008).
[116]K. Yoshimura, C. Langhammer, and B. Dam, MRS Bull. **38**, 495 (2013).
[117]K. J. Palm, J. B. Murray, T. C. Narayan, and J. N. Munday, ACS Photonics **5**, 4677 (2018).
[118]L. Xiao, Y. Ding, P. Wang, and H. Xie, Opt. Express **28**, 33106 (2020).
[119]B. Lamontagne, N. R. Fong, I.-H. Song, P. Ma, P. J. Barrios, and D. Poitras, J. Micro/Nanolithogr. MEMS MOEMS **18**, 040901 (2019).
[120]K. Mori, K. Misawa, S. Ihida, T. Takahashi, H. Fujita, and H. Toshiyoshi, IEEE Photonics Technol. Lett. **28**, 593 (2016).
[121]E. Hecht, *Optics* (Pearson Education, 2016).
[122]C. L. Giles and W. J. Wild, Appl. Phys. Lett. **40**, 210 (1982).
[123]J. C. Stover, "Optical scattering. Measurement and analysis," (SPIE Press, 1995).
[124]P. Beckmann and A. Spizzichino, "The scattering of electromagnetic waves from rough surfaces" (Artech House, Inc., Norwood, MA, 1987), p. 511.

[125]A. Spizzichino, *The Scattering of Electromagnetic Waves from Rough Surfaces*, edited by P. Beckmann and A. Spizzichino (Pergamon Press, 1963).
[126]H. C. Hulst and H. C. van de Hulst, *Light Scattering by Small Particles* (Courier Corporation, 1981).
[127]E. J. McCartney, "Optics of the atmosphere: Scattering by molecules and particles" (John Wiley and Sons, Inc., New York, 1976), p. 421.
[128]H. Chen, D. Cho, K. Ko, C. Qin, M. P. Kim, H. Zhang, J.-H. Lee, E. Kim, D. Park, and X. Shen, ACS Nano **16**, 68 (2021).
[129]Y. Jiang, S. Zeng, Y. Yao, S. Xu, Q. Dong, P. Chen, Z. Wang, M. Zhang, M. Zhu, and G. Xu, Polymers **11**, 103 (2019).
[130]S. M. Mahpeykar, Q. Xiong, J. Wei, L. Meng, B. K. Russell, P. Hermansen, A. V. Singhal, and X. Wang, Adv. Opt. Mater. **4**, 1106 (2016).
[131]D. Ge, E. Lee, L. Yang, Y. Cho, M. Li, D. S. Gianola, and S. Yang, Adv. Mater. **27**, 2489 (2015).
[132]P. Si, L. Yu, and B. Zhao, ACS Appl. Mater. Interfaces **12**, 27607 (2020).
[133]Z. Wang, W. Fan, Q. He, Y. Wang, X. Liang, and S. Cai, Extreme Mech. Lett. **11**, 42 (2017).
[134]H. N. Apostoleris, M. Chiesa, and M. Stefancich, J. Mater. Chem. C **3**, 1371 (2015).
[135]N. Hautiere, J.-P. Tarel, J. Lavenant, and D. Aubert, Mach. Vision Appl. **17**, 8 (2006).
[136]L. K. Choi, J. You, and A. C. Bovik, Proc. SPIE **9014**, 90 (2014).
[137]X. Ma, J. Q. Lu, R. S. Brock, K. M. Jacobs, P. Yang, and X.-H. Hu, Phys. Med. Biol. **48**, 4165 (2003).
[138]M. Warner and E. M. Terentjev, *Liquid Crystal Elastomers* (Oxford University Press, 2007), Vol. 120.
[139]I. Kundler and H. Finkelmann, Macromol. Rapid Commun. **16**, 679 (1995).
[140]C.-W. Chen, A. N. Brigeman, T.-J. Ho, and I. C. Khoo, Opt. Mater. Express **8**, 691 (2018).
[141]C. Meng, E. Chen, L. Wang, S. Tang, M. Tseng, J. Guo, Y. Ye, Q. F. Yan, and H. Kwok, Opt. Express **27**, 13098 (2019).
[142]H.-Y. Tseng, L.-M. Chang, K.-W. Lin, C.-C. Li, W.-H. Lin, C.-T. Wang, C.-W. Lin, S.-H. Liu, and T.-H. Lin, Materials **13**, 4137 (2020).
[143]Y. Zhang, C. Wang, W. Zhao, M. Li, X. Wang, X. Yang, X. Hu, D. Yuan, W. Yang, and Y. Zhang, Polymers **11**, 1869 (2019).
[144]S.-W. Oh, S.-M. Ji, C.-H. Han, and T.-H. Yoon, Dyes Pigm. **197**, 109843 (2022).
[145]J. Zhang, G. Pu, M. R. Dubay, Y. Zhao, and S. J. Severtson, J. Mater. Chem. C **1**, 1080 (2013).
[146]J. Y. Park, H. Song, T. Kim, J. W. Suk, T. J. Kang, D. Jung, and Y. H. Kim, Carbon **96**, 805 (2016).
[147]H. Cho, J. Kwon, I. Ha, J. Jung, Y. Rho, H. Lee, S. Han, S. Hong, C. P. Grigoropoulos, and S. H. Ko, Sci. Adv. **5**, eaav4916 (2019).
[148]J. Schroeder and J. H. Rosolowski, Proc. SPIE 0297, 156 (1982).
[149]R. Apetz and M. P. Van Bruggen, J. Am. Ceram. Soc. **86**, 480 (2003).
[150]Y. Ke, Q. Zhang, T. Wang, S. Wang, N. Li, G. Lin, X. Liu, Z. Dai, J. Yan, and J. Yin, Nano Energy **73**, 104785 (2020).
[151]J. C. Stover, *Optical Scattering: Measurement and Analysis* (SPIE Optical Engineering Press, Bellingham, 1995), Vol. 2.
[152]A. Krywonos, Ph.D. dissertation (University of Central Florida, 2006).
[153]A. Krywonos, J. E. Harvey, and N. Choi, J. Opt. Soc. Am. A **28**, 1121 (2011).
[154]C. Carniglia, Opt. Eng. **18**, 182104 (1979).
[155]J. Eastman, "Surface scattering in optical interference coatings," Ph.D Univ. of Rochester, 1974.
[156]D.-Y. Khang, J. A. Rogers, and H. H. Lee, Adv. Funct. Mater. **19**, 1526 (2009).
[157]A. L. Volynskii, S. Bazhenov, O. V. Lebedeva, and N. F. Bakeev, J. Mater. Sci. **35**, 547 (2000).
[158]P. Kim, M. Abkarian, and H. A. Stone, Nat. Mater. **10**, 952 (2011).
[159]H. Jiang, D. Y. Khang, J. Song, Y. Sun, Y. Huang, and J. A. Rogers, Proc. Natl. Acad. Sci. U.S.A. **104**, 15607 (2007).
[160]C. Harrison, C. M. Stafford, W. Zhang, and A. Karim, Appl. Phys. Lett. **85**, 4016 (2004).
[161]C. Yu, K. O'Brien, Y.-H. Zhang, H. Yu, and H. Jiang, Appl. Phys. Lett. **96**, 041111 (2010).
[162]T. Ohzono, K. Suzuki, T. Yamaguchi, and N. Fukuda, Adv. Opt. Mater. **1**, 374 (2013).
[163]M. Aschwanden and A. Stemmer, Opt. Lett. **31**, 2610 (2006).
[164]E. Lee, M. Zhang, Y. Cho, Y. Cui, J. Van der Spiegel, N. Engheta, and S. Yang, Adv. Mater. **26**, 4127 (2014).
[165]Q. Jin, Q. Zhang, J. Chen, T. Gehring, S. Eizaguirre, R. Huber, G. Gomard, U. Lemmer, and R. Kling, Adv. Mater. Technol. **7**, 2101026 (2021).
[166]M. Shrestha, G.-K. Lau, A. Asundi, and Z. Lu, "Dielectric elastomer actuator-based multifunctional smart window for transparency tuning and noise absorption," Actuators 10, 16 (2021).
[167]M. Shrestha, G.-K. Lau, A. Asundi, and Z. Lu, in *Multifunctional Smart Window based on Dielectric Elastomer Actuator* (MDPI, 2020), p. 32.
[168]J. Kim, M. Rémond, D. Kim, H. Jang, and E. Kim, Adv. Mater. Technol. **5**, 1900890 (2020).
[169]M. Shrestha, A. K. Asundi, and G. K. Lau, Proc. SPIE **10163**, 329 (2017).
[170]X. Yao, Y. Hu, A. Grinthal, T.-S. Wong, L. Mahadevan, and J. Aizenberg, Nat. Mater. **12**, 529 (2013).
[171]L. Chen, J. J. Busfield, and F. Carpi, Opt. Express **28**, 20669 (2020).
[172]M. Shrestha and G.-K. Lau, Opt. Lett. **41**, 4433 (2016).
[173]L. Chen, M. Ghilardi, J. J. C. Busfield, and F. Carpi, Sci. Rep. **9**, 20125 (2019).
[174]R. Li, Ph.D. dissertation thesis (University of Michigan, 2019).
[175]N. Li, Y. Lai, S. H. Lam, H. Bai, L. Shao, and J. Wang, Adv. Opt. Mater. **9**, 2001081 (2021).
[176]Y. H. Fu, A. I. Kuznetsov, A. E. Miroshnichenko, Y. F. Yu, and B. Luk'yanchuk, Nat. Commun. **4**, 1527 (2013).
[177]D. van den Ende, J. D. Kamminga, A. Boersma, T. Andritsch, and P. G. Steeneken, Adv. Mater. **25**, 3438 (2013).
[178]L. Hu, W. Yuan, P. Brochu, G. Gruner, and Q. Pei, Appl. Phys. Lett. **94**, 161108 (2009).
[179]W. Yuan, L. B. Hu, Z. B. Yu, T. Lam, J. Biggs, S. M. Ha, D. J. Xi, B. Chen, M. K. Senesky, G. Grüner, and Q. Pei, Adv. Mater. **20**, 621 (2008).
[180]S. Shian and D. R. Clarke, Opt. Lett. **41**, 1289 (2016).
[181]S. Shian and D. R. Clarke, Soft Matter **12**, 3137 (2016).
[182]R. Huang, Appl. Phys. Lett. **87**, 151911 (2005).
[183]M. Ochsner, M. R. Dusseiller, H. M. Grandin, S. Luna-Morris, M. Textor, V. Vogel, and M. L. Smith, Lab Chip **7**, 1074 (2007).